Centre for Geo-Information

Thesis Report GIRS-2018-05

COMBINING SENTINEL-1 SAR AND LANDSAT NDVI TIME SERIES FOR ABRUPT DISTURBANCE DETECTION ON FIJI'S MANGROVE FORESTS

Case study Tropical Cyclone Winston

Jan Pokorn

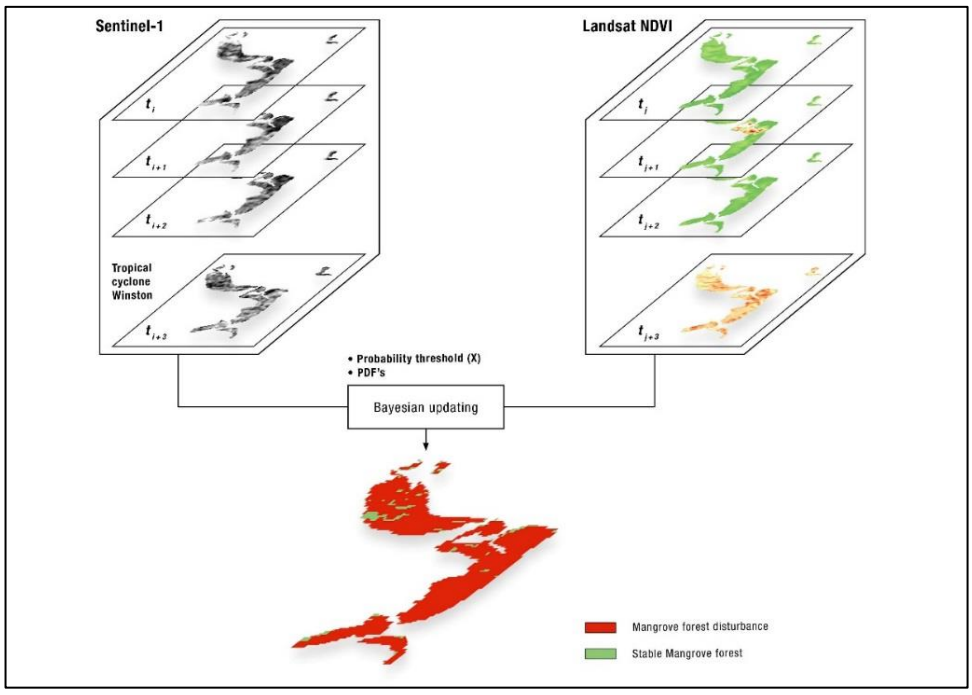

June 2018

WAGENINGEN UNIVERSITY
WAGENINGEN UR

Combining Sentinel-1 SAR and Landsat NDVI time series for abrupt disturbance detection on Fiji's Mangrove forests

Case Study Tropical Cyclone Winston

Jan Pokorn

Registration number: 91 01 29 660 050

Supervisors:

Dr. Johannes Reiche

Dr. ir. Jan Verbesselt

A thesis submitted in partial fulfilment of the degree of Master of Science
at Wageningen University and Research Centre,
The Netherlands.

Date: 14-06-2018

Wageningen, The Netherlands

Thesis code number: GRS-80436
Thesis Report: GIRS-2018-05
Wageningen University and Research Centre
Laboratory of Geo-Information Science and Remote Sensing

Foreword and Acknowledgements

'Sivi sokole, prijatelju stari,
Daj mi krila, sokole da preletim planine.
Visoka je planina, nebo iznad nje,
A na nebu sivi soko, gleda na mene.'

Peregrine falcon, my old friend,
Give me wings, so I can fly over the mountains.
The mountain is tall, the sky is above it,
And in the sky the Peregrine falcon looks upon me.

(Partisan song)

Firstly, sincere thanks to Johannes for his enthusiasm and guidance throughout the thesis process and to Jan for his useful comments. Despite the challenging topic, your in-depth knowledge on the matter always inspired me to try to improve my own skills and scientific competence.

Secondly, thanks to my family and Špela, who always stood by my side, no matter what. Additionally, I would like to thank people from the MGI – Arno, Careli, Nicolas, Samantha and Christos for countless discussions at the coffee breaks and to Willy for successfully guiding us through the master programme.

And last but not least, thanks to Wageningen. World would be a much nicer place if it resembled Wageningen just a bit more.

Table of Contents

List of Tables

List of Figures

List of Abbreviations

X(chi) **Probability threshold**

ESA **European Space Agency**

F **Stable forest**

M_{REF} **Reference period**

M_{MON} **Monitoring period**

MTL **Mean time lag**

MTL_F **Mean time lag of flagged change**

NDVI **Normalized Difference Vegetation index**

NF **Disturbed forest**

NRT **Near Real Time**

OA **Overall accuracy**

PA **Producer's accuracy**

PDF **Probability density function**

SAR **Synthetic Aperture Radar**

UA **User's accuracy**

Abstract

Mangrove ecosystems play a crucial role in the protection of coastal areas in Fiji. In addition, they are considered to be one of the largest carbon sequesters in (sub) tropical areas, playing an important role in the global carbon cycle. Therefore, conservation efforts are directed towards developing a reliable monitoring system with the capacity to detect disturbances in near real time. With the use of new medium-resolution sensors, dense time series became available for analysis, enabling timely and accurate disturbance detection. The potential of combining synthetic aperture radar (SAR) and optical datasets into dense time series for decreasing detection delays has already been proven. Here, we combined multi-temporal Sentinel-1 C-band SAR with Landsat NDVI for near real time disturbance detection after the tropical cyclone Winston. We used spatial normalization for Landsat and combined it with Sentinel-1 within a probabilistic approach. We compared the obtained results to using Landsat and Sentinel-1 separately. Our findings show that, in comparison to Landsat, using Sentinel-1 significantly decreases the disturbance detection delay due to a high observation density and a high proportion of valid observations per acquisition. In the area we used for the methodology development, using combined datasets resulted in further improvement of the temporal and spatial accuracy. We developed a thorough validation approach and created our own reliable reference dataset to compensate for the lack of field reference data. In addition, we calculated accuracy measures for different confidence levels to demonstrate the possible trade-off scenarios between the spatial and temporal accuracies depending on the user's objective. User's and producer's accuracies of the combined dataset at the highest confidence level of confirmed disturbance were 96% 89% respectively. The disturbance detection time delay was 24 days. In comparison, the disturbance detection delay when using only Sentinel-1 was 26 days, and 71 days when using only Landsat. We decided to extrapolate our methodology to an area with a larger extent (Eastern part of Viti Levu) and estimate the damage caused by the Winston tropical cyclone. Our results show that 37% of mangrove ecosystems in the study area experienced disturbance and the time delay of confirmed disturbance was 48 days. We recommend adaptations to our existing methodology for further research.

Keywords: Sentinel-1, Mangroves, Landsat, Near real time, Change detection, Forest disturbance, Tropical cyclone, Time series

1. Introduction

1.1. Mangrove ecosystems

Mangrove ecosystems are found in tropical and subtropical regions of the world between approximately 30˚N and 30˚S latitude with an estimated coverage of 137.000-152.000 km^2 (Figure 1) (Giri et al. 2011; Spalding et al. 2010; FAO 2007). Structure-wise, mangrove ecosystems are comprised of diverse trees and shrubs that exhibit common adaptive features to salinity (e.g. exposed breathing roots, stem supporting structures and salt-excreting leaves) (Ghosh 2011; Giri et al. 2011; Kuenzer et al. 2011).

Mangroves ecosystem services include: providing support to commercial and recreational fisheries, providing food, firewood and raw building materials for the local inhabitants. Furthermore, as biodiversity hotspots they represent an important habitat for unique types of flora and fauna. As they represent a transition zone between saline and fresh water, the ecosystem stabilizes the coastline by trapping debris and sediment from the surroundings and decrease sea erosion, acting as a protective buffer (Cornforth 2013; Brander et al. 2012; Atkinson et al. 2016).

Additionally, mangrove ecosystems have the capacity to mitigate consequences of natural events such as tropical cyclones or tsunamis by providing additional drag for attenuating waves and surges with their structure of trunks, leaves, root systems and unconsolidated substrate (Cougo et al. 2015; Marois & Mitsch 2015; Zhang 2013; Atkinson et al. 2016). Study on a super cyclone Odisha from Das & Vincent (2009) showed statistical correlation between mangrove presence and reduction in human deaths. Results from similar studies on sites in Thailand (Barbier 2007), Belize (Granek & Ruttenberg 2007) and India (Danielsen et al. 2005) confirmed the importance of mangrove protecting role.

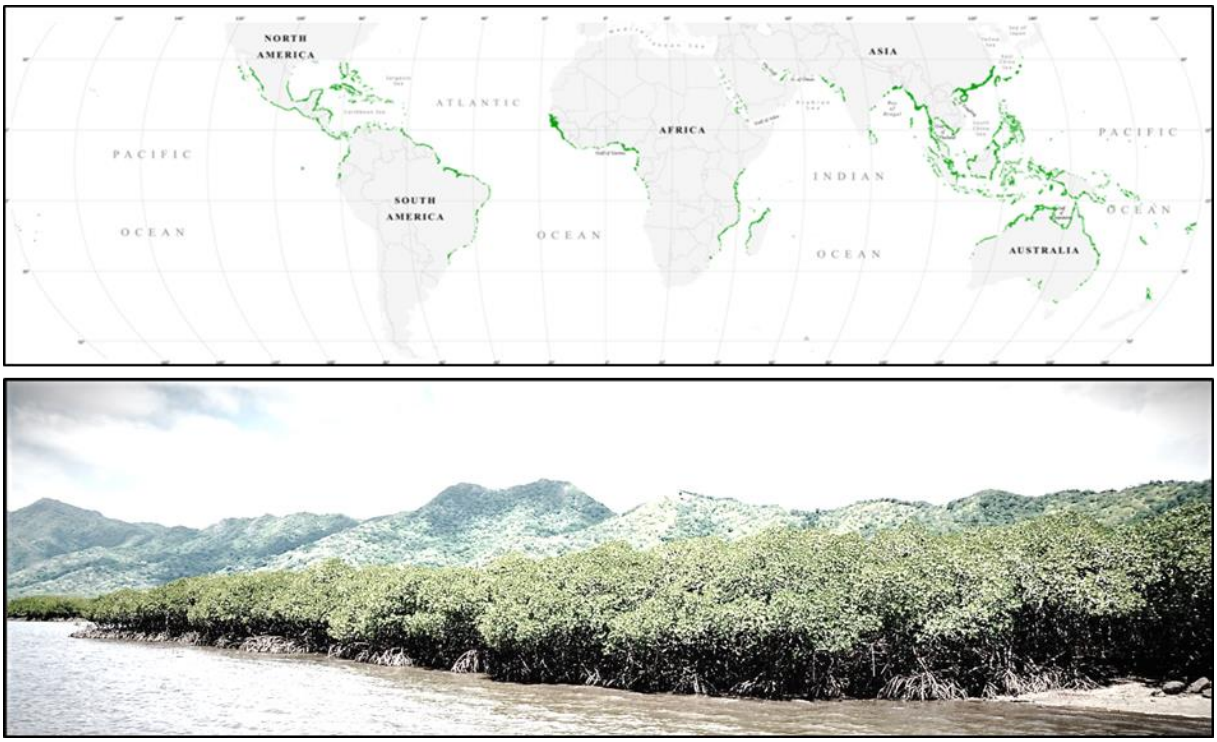

Figure 1: Global mangrove map from year 2000 (above) and Mangrove ecosystem structure (below). Source: Giri et al. (2011).

However, despite its resilience towards severe storms and occasional inundation by tides, the ecosystem is also exceptionally vulnerable to the changes in the sea-level rise and other direct/indirect anthropogenic influences (Ellison 2015).

Although there are still considerable uncertainties in the carbon balance of the mangrove ecosystem, it is considered as one of the largest carbon sequesters in (sub)tropical areas, contributing a major stake to reducing emissions in the context of global carbon cycle. Despite the awareness on the environmental importance of mangroves, urbanization, agriculture, and natural disturbances caused degradation of 35 % world's mangrove areas in the period between 1980 and 2005. Furthermore, mangrove degradation continues at 2.1% per year (Hieu 2017 Giri et al. 2016; Alongi 2008).

Consequently, many of restoration and conservation efforts have been undertaken to address the issue under the support of international treaties and conventions (e.g. Ramsar convention and Kyoto protocol) (Hieu 2017; Kuenzer et al. 2011; Ramsar convention 2017).
One of the major challenges next to implementing sustainable management is addressing the inter-dependencies between disturbance processes and complex climate change factors (e.g. rise in CO_2 levels, air temperature increase, sea level rise), which alter the function and state of the mangrove ecosystem (Cohen et al. 2017; Ward et al. 2016).

Disturbance processes can be divided in two groups (Cohen et al. 2017, Alongi 2008):

1. Discrete events of high-impact (e.g. fires, seismic activity, cyclones, logging) which drastically change ecosystem state.

2. Gradual processes that require years to decades to evolve and reach full extent (e.g. diseases, air pollution).

This study focuses on detecting damages on mangrove ecosystems following a discrete disturbance – Tropical cyclone.

Tropical cyclones are one of the most important natural disturbances impacting the structure, function and dynamics of mangrove ecosystems. The main driver behind resulting damage is primarily wind speed. Although strong winds are the cause for the most of the structural damage on mangrove ecosystems, the damage extent additionally depends on mangrove type and peculiar characteristics (e.g. tree size, species composition, stand properties and topography) (Negron-Juarez 2014; Lugo 2008).

1.2. Mangrove ecosystems monitoring using remote sensed data

In the past, aerial photography was largely the only source for estimating extent and condition of world's mangroves. To the present day, aerial imagery is a reliable source of information for local and regional extents and is used for change detection, habitat-management support and assessment of classification procedures on lower-resolution sensors. Furthermore, it is the only source of information that enables long-term time series analysis >50 years (Kuenzer et al. 2011; Giri et al. 2011; Purnamasayangsukasih et al. 2016).

For the last three decades, availability of medium resolution sensors enabled development of change detection applications for mangrove ecosystems. Landsat TM and SPOT have been extensively used in combination with visual interpretation and digitalization (Kuenzer et al. 2011; Long et al. 2013; Kanniah et al. 2015). Launch of high resolution satellites IKONOS-2 and Quickbird in 1999 and 2001, respectively, opened new opportunities for mangrove mapping with improved identification on species level (Kuenzer et al. 2011; Giri et al. 2011).

Airborne and spaceborne radar sensors were used in numerous studies on structural parameters (Proisy et al. 2002), health status (Kovacs et al. 2006; Kovacs et al. 2008) and biomass mapping (Proisy et al. 2003). Special attention was given to the differences in backscatter between canopy structure, frequencies (C-band, L-band, P-band) (Table 1) and different polarization modes (HH, VV, HV).

C-band	L-band
Penetration into the upper part of the canopy, few meters within the crown	Deeper canopy penetration, involving scattering from trunks and ground surface
Interaction with leaves and small branches	Volume scattering predominates by interaction with multiple branches of various sizes
Increase in backscatter is indicative of changing forest structures	Increase in backscatter is indicative of changing forest structures
Sensitive to crown characteristics (number, density, size and leaf orientation) and canopy structure (architecture and heterogeneity)	Double-bounce scattering between trunks and ground
	Sensitive for biomass

Table 1: Comparison of mangrove ecosystem properties in radar C-band and L-band. Adapted from Kuenzer et al. (2011).

1.3. Near Real Time forest disturbance monitoring using remote sensed data

For a quantitative assessment of ecosystem disturbances, data acquired before and after the forest change is essential. Since events as tropical cyclones or tsunamis are largely unpredictable in space and time, field data acquisition before the event is nearly impossible. On the other hand, gathering the field data after natural disasters is feasible, but time and resources consuming. Additionally, in case of mangrove ecosystems, accessibility for surveying is logistically limited due to its structure (Zhang 2013; Granek & Ruttenberg 2007).

Therefore, the use of Remote Sensing is essential as a cost-effective method to monitor forest change and subsequently assess the damage (Griffiths 2015). With the availability of new medium resolution sensors (e.g. Sentinel-1, Sentinel-2, Landsat 8), dense time-series became available for detailed analysis. Monitoring of disturbances for damage evaluation and policy making has recently relied on optical sensors due to easier processing of the data, continuity (e.g. Landsat, MODIS) and easier interpretation (Reiche 2015; De Sy et al. 2012; Kanniah et al. 2015). In mangrove ecosystems, however, temporal and spatial accuracy of the optical data is often affected by missing values due to frequent cloud cover in (sub)tropical areas.

Using SAR (Synthetic Aperture Radar) addresses the lack of cloud-free observations with two major advantages over optical data; it is capable of data acquisitions under most weather conditions and independent of sunlight, which makes it useful for monitoring disturbances (Chen 2016; Reiche 2015). Recently, combining SAR and optical data has been the focus of numerous scientific studies, exploiting benefits of multiple data sources for applications of land cover/land use (LULC) mapping (Herold & Haack 2008; Sheoran & Haack 2013; De Oliveira Pereira et al. 2013), crop inventory (McNairn et al.

2009) and forest monitoring (Lehmann 2015; Reiche 2015; Thomas et al. 2015). Specific interest is shown towards the key advantages of data interoperability (obtaining the same thematic result with two or more sensors) and complementarity (enhancing thematic value by using multiple sensors) (Lehmann 2015, Kuenzer et al. 2011).

All of the above mentioned applications address complementarity and partly change detection. However, when a natural disturbance event occurs, the resulting damage needs to be addressed as soon as possible to minimize resources, needed for the post-disaster recovery period. With an appropriate monitoring system, forest managers and environmental organizations would be able to get information in the shortest possible time lag and design appropriate plan for ecosystem regeneration.

A novel Bayesian approach for exploiting the full potential of SAR in combination with optical sensors for detecting deforestation was proposed by Reiche et. al. (2015). The method proved to be successful in decreasing time lag between a deforestation event and deforestation detection. Reiche et al. combined data from optical Landsat NDVI and radar ALOS PALSAR L-band sensors, using Bayesian approach for NRT (near real-time) monitoring. The proposed monitoring system is designed to use inputs from multiple optical or/and radar sensors and is orientated towards disturbance detection in tropical areas. Functional monitoring system would not only contribute to significant temporal and spatial accuracy improvement with damage assessments following natural disasters, but with minor adjustments also provided us with potential small to medium scale illegal logging locations in NRT.

As a part of ESA's (European Space Agency) Copernicus programme, Sentinel mission is an operational Earth Observation program, that provides global information in domains of land, marine, atmosphere, emergency response, climate change and security monitoring applications (Nagler 2015). Sentinel-1 is the first operational of the six missions in Copernicus programme. It is composed of two polar-orbiting satellite constellations, equipped with SAR sensors, measuring in C-band; Sentinel-1A and Sentinel-1B, launched in April 2014 and April 2016 respectively (Torres 2012). With Sentinel constellation of satellites, consistent and reliable long-term data archive based on dense time-series is becoming available for environmental monitoring applications, one of them being monitoring mangrove ecosystems in NRT.

1.4. Problem definition

Multiple monitoring approaches for detecting forest disturbances are available and can be divided in two groups, according to the capacity of the system to detect change in a satellite image once it is available. First group consists from monitoring systems, designed for detecting disturbance on annual and sub annual level, using data from a single sensor. The second group is focused on disturbance detection in near real time (NRT) and enables quick response.

In this study, the Bayesian approach for NRT monitoring, proposed by Reiche et al. (2015) was adapted and implemented, with combining optical $Landsat_{NDVI}$ and radar Sentinel-1 SAR C-band datasets. The approach itself has only been implemented with radar ALOS PALSAR L-band data and only on tropical forests so far (Reiche 2015). Research effort in our study is solely directed towards disturbance detection on coastal mangrove ecosystems with C-band SAR.

In comparison with L-band sensors, Sentinel-1 SAR C-band is much less susceptible for disturbance detection in mangrove ecosystems (Kuenzer et al. 2011; Reiche 2015). L-band penetrates deeper into the canopy than C-band and consequently the contrast between disturbed and undisturbed mangrove ecosystems is larger (Woodhouse 2006; Kuenzer et al. 2011; Mitchell et al. 2014; Reiche 2015).

However, dense Sentinel-1 dataset has the potential to improve mangrove loss detection compared to the L-band due to numerous observations per month.

To address the challenge of validating our methodology without any field reference data, emphasis is given on using a set of "good practice" recommendations for implementing accuracy assessment of the result, by deriving our own reference data from independent satellite imagery (Olofsson et al. 2014).

In the study, Sentinel-1A SAR C-band and Landsat 8 $_{NDVI}$ datasets were used to explore and assess the benefits of combining dense time-series from multiple sensors in the scope of timely damage detection on Fiji's mangrove ecosystems following Winston cyclone event.

If the method proves reliable, further applications for disturbance monitoring are possible with additional analysis steps (e.g. illegal logging, forest fires, damage from tsunami), providing valuable information on mangrove ecosystems disturbances.

1.5. Research objective & Research questions

The thesis objective is to combine time series data from Sentinel-1 SAR C-band and Landsat 8 optical sensor for detecting mangrove forests disturbance following the Winston cyclone and at the same time improve spatial and temporal accuracy for detecting disturbance compared to a single sensor.

I. What are the capabilities of dense Sentinel-1 C-band SAR time series and optical Landsat NDVI time-series datasets to detect disturbances in mangrove ecosystems on Fiji?

II. Can we improve spatial and temporal accuracy of disturbance detection in mangrove ecosystem by combining Sentinel-1 and Landsat NDVI time series?

III. What is the damage extent on mangrove ecosystems in the study area?

Mangrove ecosystems are from here on referred to as forests for the clarity of the report.

2. Study area & Data

2.1. Study area, Development area and Winston tropical cyclone

- *Study case: Tropical cyclone Winston*

On February 19, 2016, Fiji was struck by a category 5 tropical cyclone Winston with wind speeds reaching 300 km/h, thus being one of the strongest cyclones ever recorded in the Southern Hemisphere (Le Page 2016). It travelled between two of the biggest islands Vanua and Viti Levu, damaging substantial northern and southern parts on the, respectively (Di Liberto 2016). In Fiji, cyclones with wind speeds of 150 km/h may be expected every 5-10 years, cyclones with 200 km/h every 30-50 years and those of 250 km/h and more once in a few centuries in (Ash, 1992).

- *Development area*

The development area is comprised of forests next to Viti Levu Bay, situated in the North-Eastern part of the island (Lat. 178.25° S, Lon. 17.47° E), where the tropical cyclone Winston passed and according to Fiji's Forestry Department resulted in substantial damages on coastal forests. The impact is visible on most of the post-event image acquisitions of Landsat, Sentinel-1 and available high resolution optical datasets.

- *Study area*

The study area was selected based on Fiji's Forestry department damage reports and the Winston cyclone path. It consists of the eastern half of the Viti Levu island and coincides with the Landsat tile (path 74, row 72).

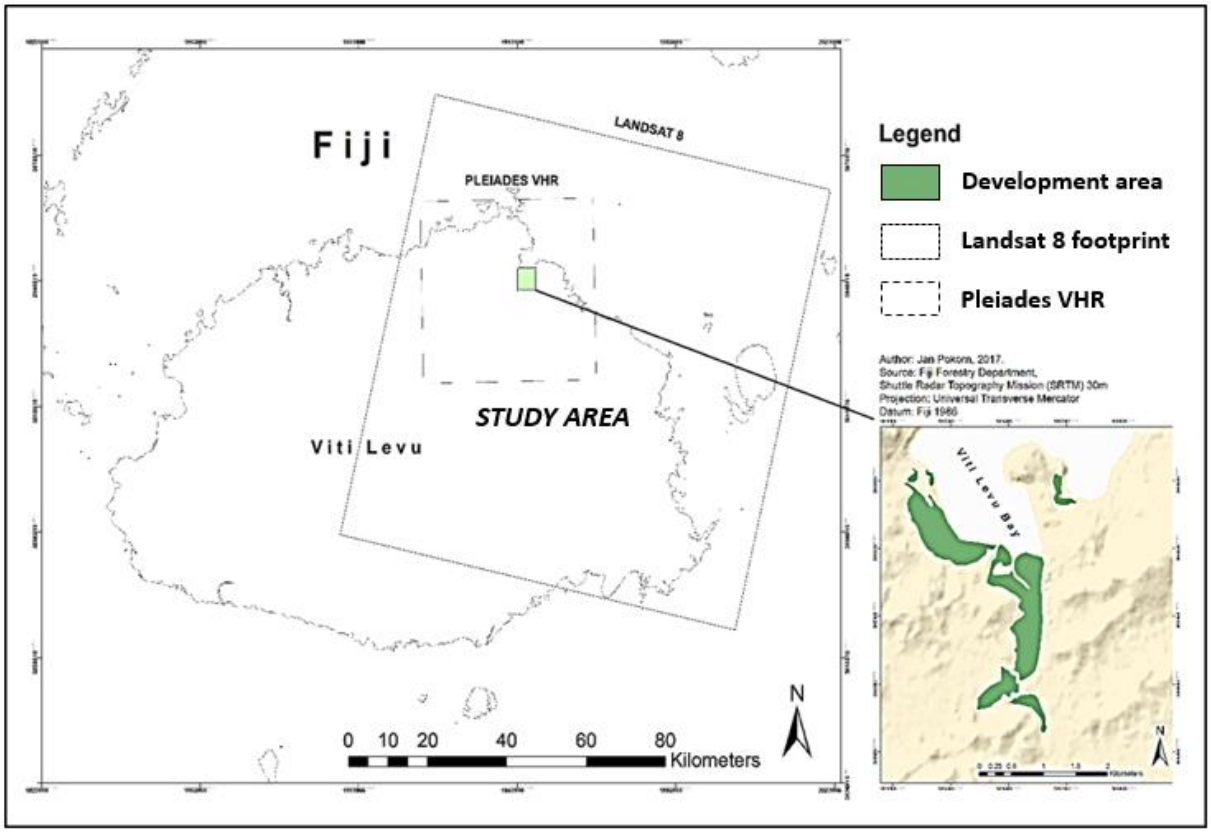

Figure 2: Development & Study area.

Figure 3: Example of Winston damage on mangrove ecosystems northern from our study area,near Rakiraki river. Source: UNICEF, 2016.

2.2. Data

Two pre-processed remote sensed datasets were provided for this study. There were significant differences between both datasets in total number of observations and number of valid observations (Figure 4).

- *Sentinel-1*

Sentinel-1 C-band Synthetic Aperture Radar (SAR) VV-polarized raster stack
Spatial resolution: 30 m.
Time span: 03/10/2014 - 05/08/2016

- *Landsat 8 NDVI*

Normalized Difference Vegetation Index (NDVI) raster stack
WRS: path 74, row 72
Spatial resolution: 30 m
Time span: 20/05/2013-16/08/2016

- *Reference data*

For the purposes of the master thesis, multispectral VHR (Very High Resolution) data with spatial resolution of 2 metres was provided from Pleiades satellite (extent provided in Figure 2). Freely available Worldview 2 imagery from before the disturbance event (2015) and Planet Labs imagery from after the event was used. Additionally, digital elevation model (SRTM) with 30m resolution was provided for taking Sentinel-1 topographical anomalies into consideration with the method development.

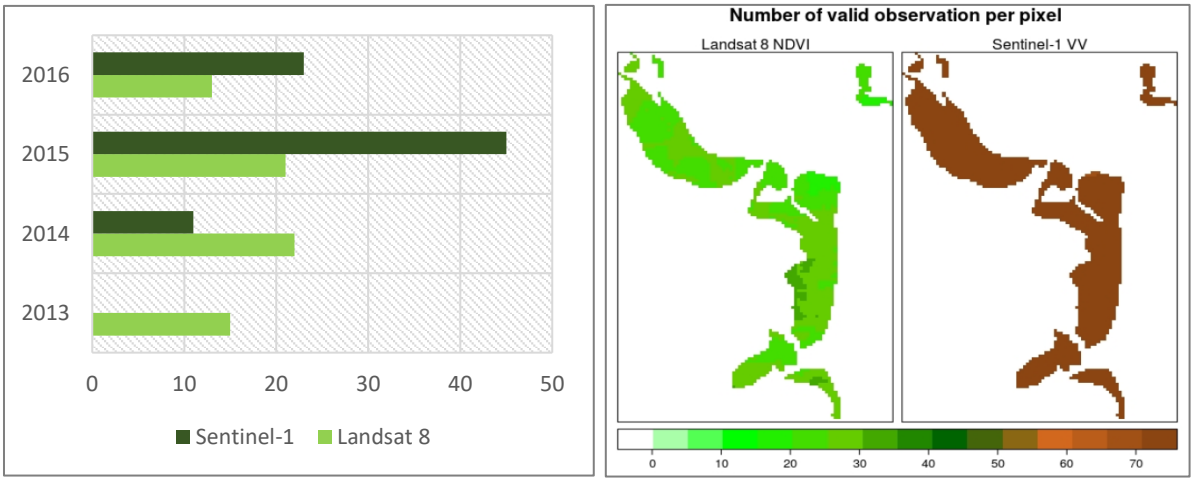

Figure 4: Left: Number of total Landsat and Sentinel-1 observations per year in the development area. Right: Two maps represent the number of valid sensor observations per pixel from 2013 onwards. Here, a valid observation stands for every pixel that has a value.

3. Methods

3.1. Overview & Methodology flowchart

The research methodology is comprised of three major parts, with the first two conducted for the development area and the third one for the entire study area:

- Separability analysis **(Research question 1)**
- Applying the Bayesian approach for disturbance detection. The method was validated temporally using Time Sync approach and spatially using error (confusion) matrix **(Research question 2)**
- Methodology was later extrapolated to create a disturbance map for the complete study area **(Research question 3)**

Methodology and validation steps were developed and executred in R programming environment and visualized with Esri ArcGIS and QGIS software.

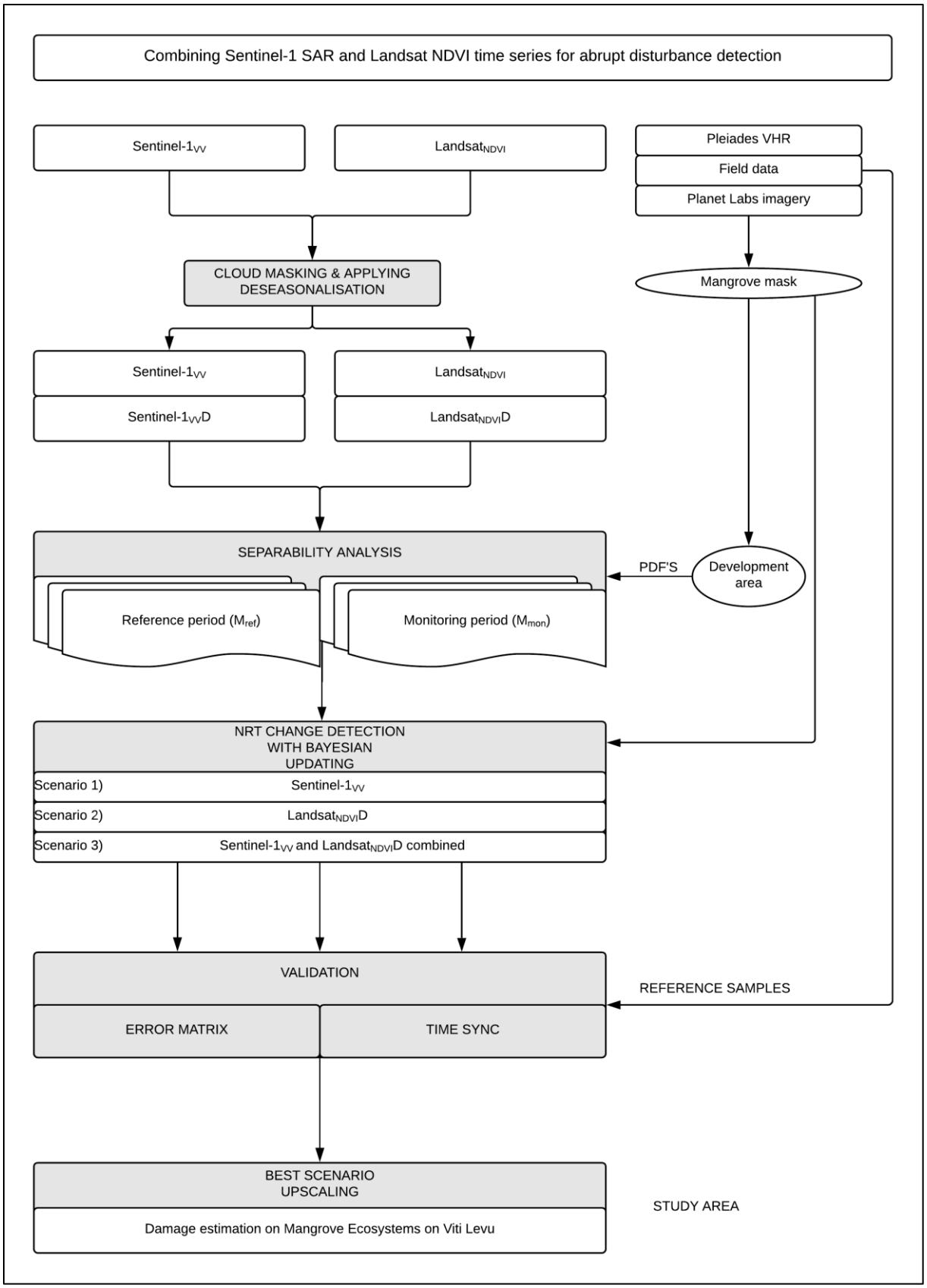

Figure 5: Methodology flowchart.

3.2. Cloud masking

Cloud mask had to be applied to the Landsat NDVI dataset ($Landsat_{NDVI}$), using package Fmask in R, to remove the remaining clouds.

3.3. Creating mangrove dataset

Areas of coastal mangrove forests were first manually digitized and NA values were given to areas outside the polygons to create a mangrove mask (F_M). All mangrove forests on the island of Viti Levu were digitized using Fiji's Forestry Department field reference dataset, Pleiades VHR and Planet Labs imagery, temporally overlapping with M_{ref}. Firstly, Forestry Department dataset was used as reference for training on the visual mangroves characteristics in high resolution imagery. Secondly, conservative decision was made to leave out the border areas, where mangrove forests transit to another forest type and exclude water bodies to ensure our produced Mangrove mask values yield actual mangrove signal/backscatter (Figure 6, right). Created forest mask was then compared to SRTM to find anomalies. Last step was rasterizing the created dataset as a required input for the Bayesian updating (see section 3.6).

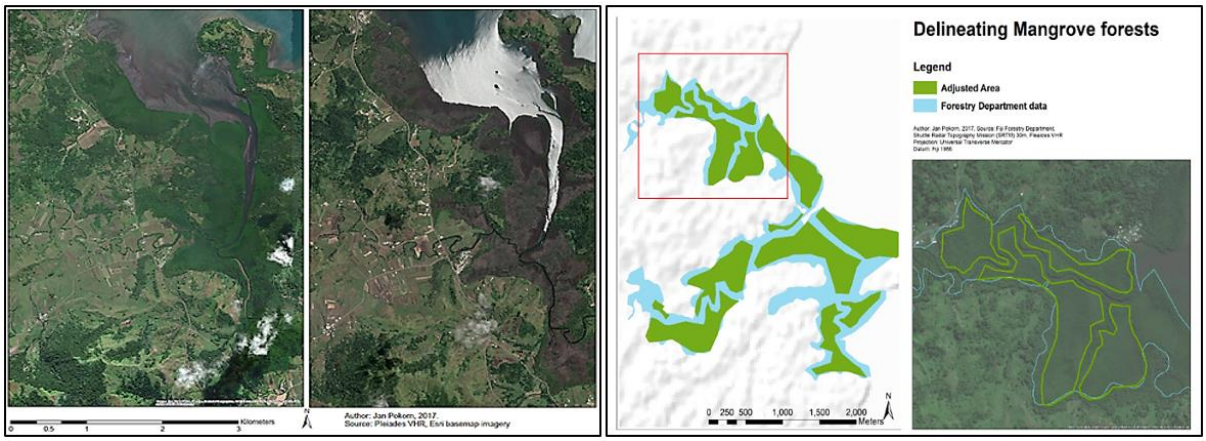

Figure 6: Left: Worldview-2 imagery (Mref, 19-09-2014) on the left and Pleiades VHR imagery (Mmon, 21-09-2016) on the right. Right: Adapting Fiji's Forestry Department Mangrove forests dataset.

Outlining an area that had clear differences between M_{ref} and M_{mon} visible in satellite imagery was also a necessity for validation part of the thesis; available Pleiades VHR imagery covered only a part of the island (see Figure 2).

3.4. Spatial normalization for reducing seasonal variation

Seasonal variation in annual forest photosynthetic activity and moisture content of the canopy are one of the main challenges affecting accurate and timely detection from remote sensed data. While photosynthetic activity affects time-series derived from optical sensors and has no measurable impact on radar datasets due to radar signal characteristics, variability in moisture content has to be taken into account for the latter (Reiche et al. 2017; Hamunyela, Verbesselt & Herold 2016). Spatial noralization can be accounted for by subtracting the spatial unit (pixel) value with the 95^{th} percentile, computed in the pixel neighborhood. The approach follows assumption that the upper part of the distribution represents forest pixels (Reiche et al. 2017). We applied spatial normalization (deseasonalization) to both pre-processed datasets ($S\text{-}1_{vv}$, $L8_{NDVI}$), to take possible seasonal trends into account and produced two additional datasets, in what follows $S\text{-}1_{vv}D$ and $L8_{NDVI}D$.

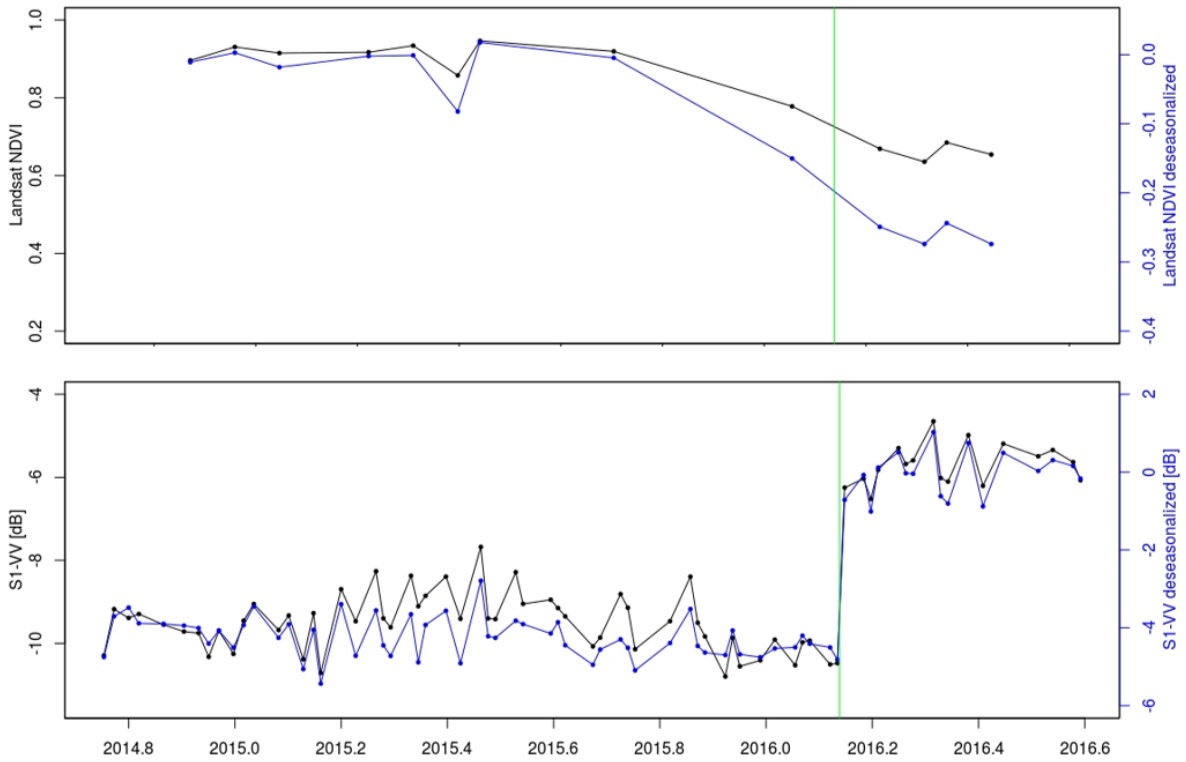

Figure 7: Original and spatially normalized time-series for LandsatNDVI and Sentinel-1VV (example from our study area, green line denotes time of the disturbance event: February 19th, 2016). The increase in backscatter[dB] with Sentinel-1$_{VV}$ time series is indica

3.5. Separability analysis

Separability analysis was done to assess, how well can a sensor discriminate between F/NF classes. Probability density functions were derived for each class separately and then compared with Jeffries-Matusita (J-M) distance measure, ranging from [0-2], with 2 being the absolute separable and 0 inseparable (Reiche 2015; Hamunyela 2017).

Probability density functions (PDF's) for stable forest and disturbed forest classes were derived separately for all four main datasets (see section 3.4). The four time series were split to reference (M_{ref}) and monitoring (M_{mon}) periods, where the M_{ref} included temporally overlapping observations taken before the tropical cyclone event (2016-02-19) and M_{mon} the observations after the event. Observations from M_{mon} were labelled as stable forest (F) and observations in M_{ref} as disturbed forest.

For deriving PDF's, a subset from our development area was selected and digitized. We focused on selecting a homogenous area with disturbance clearly visible on post-event Pleiades VHR imagery to achieve the optimal results.

Gaussian model was fitted separately for each of the F and NF distributions for the four main datasets by maximum likelihood fitting following Reiche (2015). PDF parameters (mean and standard deviation) for F and NF were later extracted for each dataset and used for estimation of the separability between stable and disturbed forest classes. We evaluated the normalized Jeffries Matusita (J-M) distance analysis and addressed RQ1. Datasets with the highest J-M distances between F and NF classes were selected for further analysis; namely Landsat$_{NDVI}$D and Sentinel-1$_{VV}$, with distances 1.83 and 1.71 respectively (Table 2).

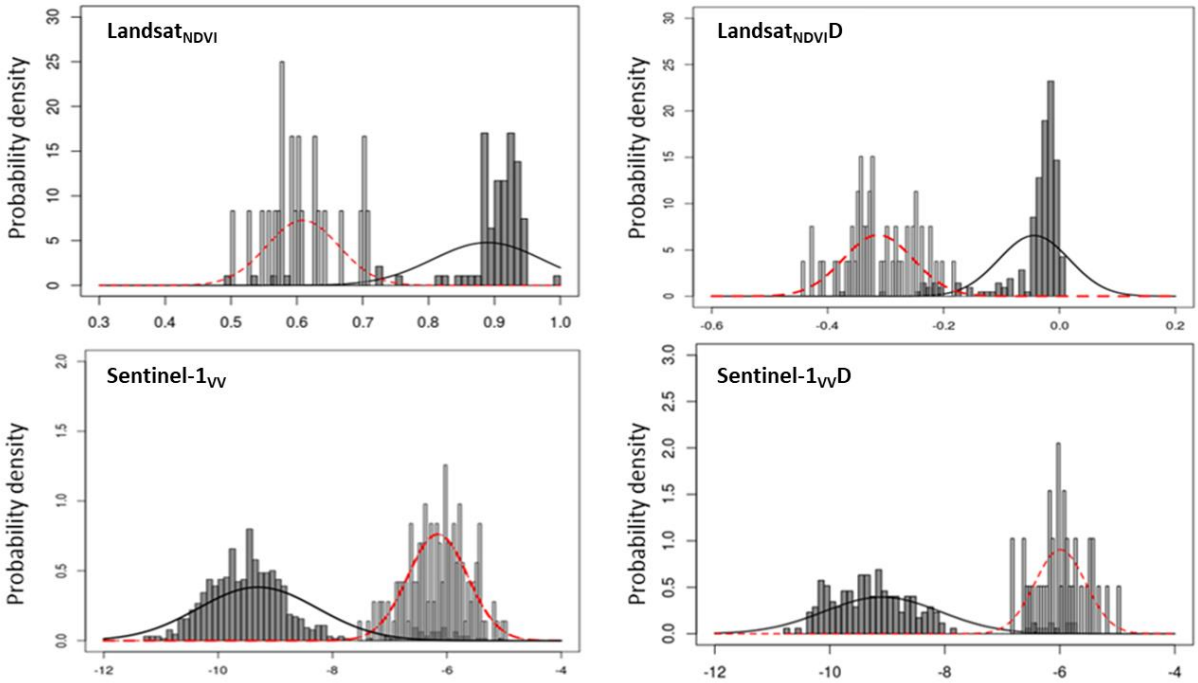

Figure 8: Extracted Probability densities for F and NF classes, with and without applied spatial normalization.

	J-M	*mean(F)*	*mean(NF)*	*std(F)*	*std(NF)*
Landsat$_{NDVI}$	1.71	0.88	0.60	0.09	0.05
Landsat$_{NDVI}$D	1.83	-0.04	-0.31	0.06	0.06
Sentinel-1$_{VV}$	1.71	-9.30	-6.16	1.04	0.52
Sentinel-1$_{VV}$D	1.66	-3.32	-0.44	0.94	0.57

Table 2: Results from the separability analysis (Jeffries-Matusita distance, mean values and standard deviation)

3.6. Using the Bayesian approach for NRT disturbance detection

The Bayesian approach proposed by Reiche (2015) enables us to exploit the benefits of using multiple time series from diverse sensors through conditional probabilities. Figure 9 illustrates the methodology with the use of two sensors, where s1 and s2 stand for sensor 1 (e.g. Landsat$_{NDVI}$) and sensor 2 (e.g. Sentinel-1$_{VV}$) and *t* refers to the distance in time between the current and any past or future observation.

First, sensor specific forest (F) and disturbed forest ecosystem (NF) probability density functions (PDFs) are used to estimate the conditional probabilities of NF for every individual time series of the two sensors (past, current, future). After that, observations at *t* are flagged for potential deforestation, if the conditional probability of deforestation is ≥ 0.5. When the observation is flagged as a potential

disturbance, Bayesian iterative updating takes into account previous observation, current observation and future observations to either confirm or reject a disturbance event at *t.*

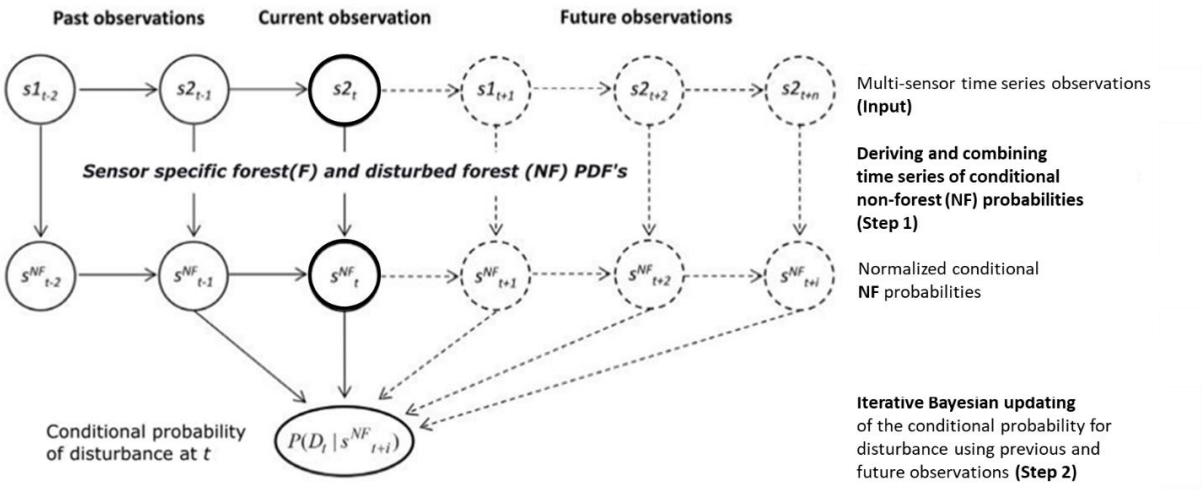

Figure 9: Schematic overview of Bayesian updating. Adapted from: Reiche et. al. (2015).

After performing the separability analysis and deriving J-M distances for multiple time-series, results showed that Sentinel-1_{VV} and Landsat$_{NDVI}$D datasets were the optimal choices for differentiating between stable and disturbed forests. Therefore, we used the above mentioned datasets as inputs to the Bayesian iterative updating.

Before running the analysis, extents of datasets for both datasets had to be harmonized – we cropped the bigger extent (Sentinel-1_{VV}) with the smaller one (Landsat$_{NDVI}$D). In the same step, we determined the initial input parameters. Start and end time were set at 2016.1 and 2016.5, respectively. This was done to exclude possible unknown events before the Winston Cyclone, which could later influence the analysis results. Thresholds (X) of 0.5, 0.6, 0.7, 0.8, 0.9 were used for detecting the disturbance (Figure 10; Appendix, Figure 17). If the conditional probability of a pixel being disturbed exceeded the used threshold in the monitoring period, pixel was labelled as disturbed forest and time of disturbance was noted down as $t_{confirmed}$.

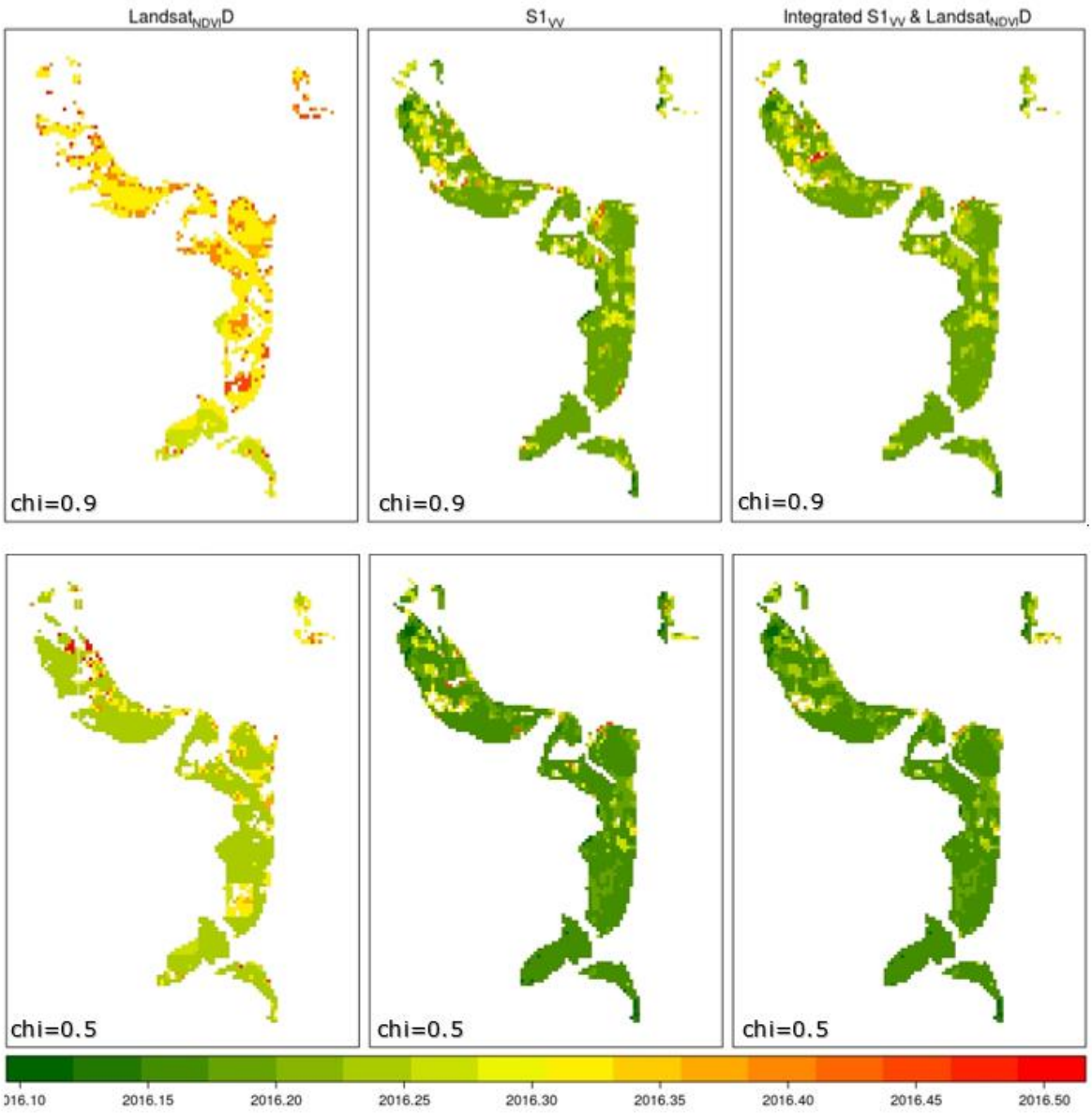

Figure 10: Results of disturbance detection with Bayesian approach for all three scenarios, showing thresholds of 0.9 and 0.5, respectively. Every pixel that has a value was confirmed for disturbance. Time of confirmed change 2016.30 corresponds to 36th day of the year and 2016.50 corresponds to 182nd day of the year.

After applying the Bayesian approach for disturbance detection in the development area, validation was performed (see section 3.7) for the three scenarios and the optimal one was selected for upscaling the methodology and input parameters to the whole study area. Additional steps of dividing the study area into multiple subsets and mosaicking them back together were needed to account for the large extent due to the limitations of the used algorithm.

3.7. Developing Validation approach

Time sync and Error matrix methods were used for assessing spatial and temporal accuracy available data. Spatial and temporal accuracies were compared, first with single sensors time series and with the two of them combined, using stable forest (F) and disturbed forest (NF) strata as reference areas for assessment of commission errors, omission errors and overall accuracies.

3.7.1. Sampling design

In the study, stratified random sampling was used and adapted according to "good practice" recommendations from Olofsson et al. (2014). Advantage of the above mentioned sampling design is that allows sample size specification, allocated to each stratum, according to the strata proportion (W_i). Therefore, sample size allocation to less represented classes (e.g. stable forest in our study) results in decreasing class accuracy standard error (Olofsson et. al, 2012). Findings from Olofsson et al. (2010, 2011) show that stable classes are more accurate, hence the desired user and producer accuracy is higher for stable classes.

Firstly, sample size per strata had to be determined according to the size of the study area and desired accuracy. Olofsson et al. (2014) worked with areas of large extents (n > 100.000 spatial units), consequently the number of validation samples to reach the desired user's accuracy in areas with smaller extents had to be adapted accordingly (otherwise the total number of samples per strata could account for more than half of the total pixels in the area). User then has to decide for one of the n-produced maps, which he assumes most accurate for allocating samples per different map strata. When working with rare classes (e.g. deforestation or other disturbances), the recommended practice is to allocate at least 50 samples per strata.

3.7.2. Sample allocation

Following methodology from Olofsson et al. 2014, we divided our development area into two groups (strata), namely stable forest (F) and disturbed forest (NF).based on the classification map, derived from scenario 3 (combined $Landsat_{NDVI}$ and Sentinel-1_{vv}). The latter scenario was chosen based upon assumption of most accurate strata division before the validation. Number of samples per strata was determined according to the size of our study area and desired accuracy outcome. Olofsson et al. were working with areas of large extents (n > 100.000 spatial units), therefore the number of validation samples to reach the desired user's accuracy in our study area had to be adapted accordingly (otherwise the total number of samples per strata would account for half of the total pixels in the area). We therefore decided to use 1/5 of recommended samples and allocate 210 samples in total 150 to areas, classified as disturbed forest (NF) and 60 samples stable forest (F), respectively. Sample allocation was done using sampleRandom function in R, which allocates random raster cells without a replacement per strata. The derived samples were then compared to the reference data as described below.

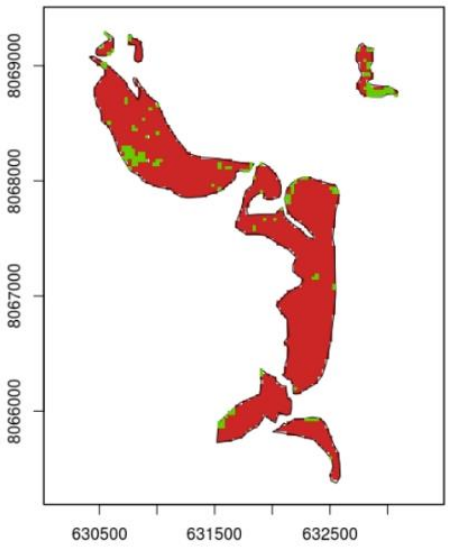

Figure 11: Initial Stable forest strata (green) and disturbed forest strata(red), used for sample allocation in the development area.

	Strata proportion (Wi)	***Allocation***
Disturbed forest strata (NF)	0.934	150
Stable forest strata (F)	0.066	60

Table 3: Proportion of classified F and NF areas & number of allocated samples per strata.

3.7.3. Creating reference dataset

First step towards creating a reliable reference dataset was visual evaluation of individual samples, displaying complete time series of $Landsat_{NDVI}$ per pixel. The $Landsat_{NDVI}$ was used for decision making based on easier interpretation in comparison with Sentinel-1_{vv} and with regards to the large number of sample time series we had to analyze (Kasischke et al. 1997; Kuenzer et al. 2011).

In addition, high resolution imagery was used for easier interpretation. After browsing through reference samples, decision was made to quantify a threshold of change (ϑ) and use the following decision rules for determining of F and NF based on $Landsat_{NDVI}$ time series and additional visual analysis of high resolution imagery:

I. *Since the exact time of the event is known, the two consecutive observations that are being evaluated must be the **last** observation before the event and the **first** observation after it. In case an observation coincides with the time frame of the event [+-2 days], the previous observation was evaluated.*

II. *If $\vartheta \geq 0.2$ for the last and first observation, we additionally checked the first observation after the event for outliers (single values exceeding the threshold ϑ with steep increase after the observation). In case there were no outliers we labeled it as NF, else we labelled it as F (figure 12).*

III. *When the change is visible in the satellite imagery and $0.2 \geq \vartheta \geq 0.19$, decision is made based on testing that was done with time series analysis.*

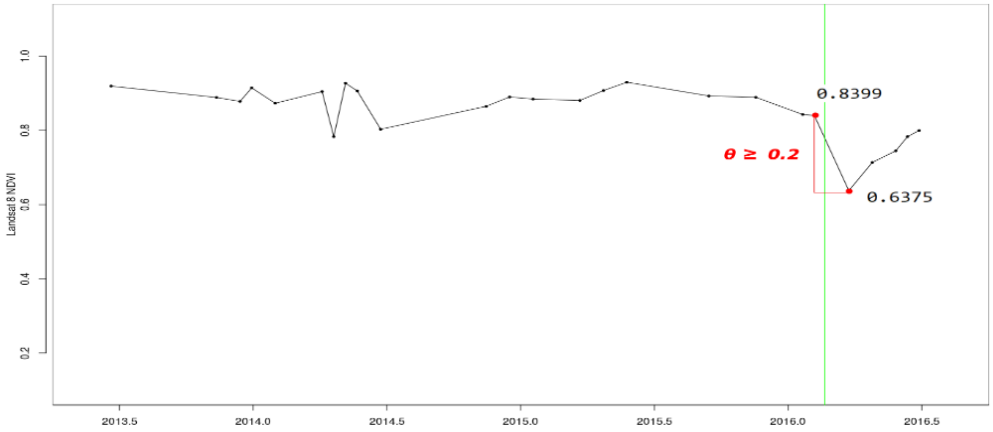

Figure 12: Example of steep increase of LandsatNDVI values after the event with θ ≥ 0.2. Pixel was labelled as stable forest (F).

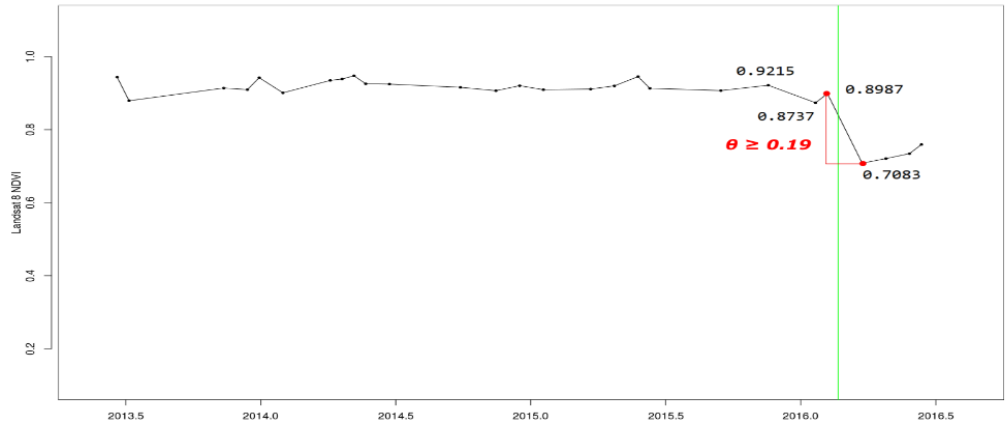

Figure 13: Example of analyst decision with 0.2 ≥ θ ≥ 0.19; reference sample was labelled as disturbed forest (NF).

After the decision was made for each sample separately, corrected, more reliable reference dataset was derived for validation with modified number of spatial units per strata (see Table 4; sample allocations in appendix - tables 5 & 6). The new reference was used for the validation of all the derived maps.

	Strata proportion (Wi)	***Allocation***
Disturbed forest strata (NF)	0.934	121
Stable forest strata (F)	0.066	89

Table 4: Sample allocation after deriving a new reference dataset.

3.7.4. Spatial accuracy

Binary Error (Confusion) matrix is a common cross-tabulation method, used in Remote sensing to quantitatively assess measures of change and change detection accuracy (FAO 2016).

Figure 14 shows elements of the matrix. As this is a common method for estimating accuracy in remote sensing applications, only 2 classes are used for simplification, however the same procedure applies to classification maps with n-classes. Map units, classified as change (N_{11}) and no change (N_{22}) are labelled as true positives and true negatives, respectively. These units represent correctly classified pixels per class, while N_{21} (no-change) and N_{12} (change) stand for false negatives and false positives, so called misclassified pixels.

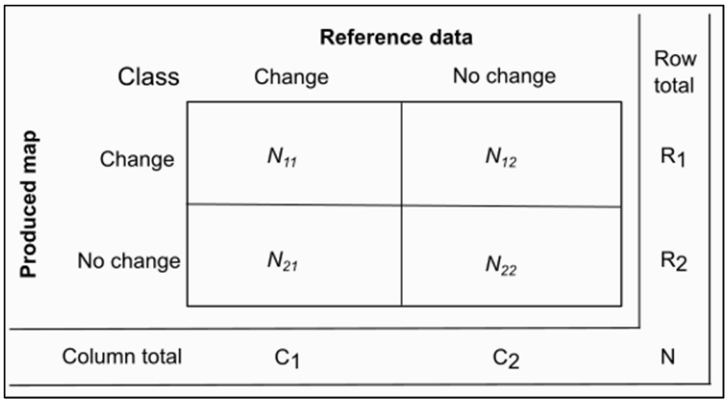

Figure 14: Error matrix with change and no change classes of reference data and the produced map. Adapted from (Bogoliubova & Tymkov 2014).

N represents total number of classified pixels and is derived as rows or columns sum.

$$N = \sum Ri = \sum Ci$$

We can express measure for the overall classification accuracy (*OA*) in percentages from the error matrix by summarizing correctly identified pixels (M_i) and dividing it by the total number of pixels (*N*). The result has to be multiplied by 100 to yield a value as a percentage.

$$OA = \frac{\sum Mij}{N}$$

The producer's accuracy (PA) is computed as all correctly classified pixels of a given class (T_i), divided by the total number of pixels in that same class (R_i). Omission error is derived as 1 - PA and it yields probability that spatial unit classified as category *k* in the reference data represents category *k* in the produced map (FAO, 2016).

$$PA = \frac{Ti}{Ri}$$

The user's accuracy (UA) is a map-based accuracy, which represents a fraction of correctly classified map pixels with regard to all pixels, classified as the same class in the map. Commission error is derived as 1 – UA (FAO, 2016).

$$UA = \frac{Ti}{Ci}$$

3.7.5. Assessing temporal accuracy

Time Sync method, proposed by Cohen et al. (2010) is used to create a reliable reference dataset. Time Sync is a visualization and data collection tool, developed to accommodate veracity of output from time series. User goes through pixels of co-registered imagery, acquired after the event, detecting change in pixel values for previously defined stable forest/disturbed forest areas. When a change in pixel is detected (potential disturbance), results are compared to our monitoring system and temporal accuracy is derived from the time lag between user visual detection and detection with the Bayesian approach. The additional value of Time Sync is the sampling design flexibility. Usually validation methods use temporal and spatial subsets of the whole dataset, while Cohen's method evaluates every available image and provides us with the needed temporal detail for our application (Cohen et al. 2010).

We estimated the temporal accuracy by calculating mean time lags (MTL) between the disturbance event (Tref) and the time of the confirmed disturbance (Tcon). We additionally calculated mean time delay (MTL_F) between Tref and when the confirmed disturbance event was initially flagged.

4. Results

4.1. Area adjusted spatial and temporal accuracies for our study area

Validation results for the three scenarios were compared for stable forest (F) and disturbed forest (NF) (Appendix, Table 7). Threshold values (*X*) [0.5, 0.6, 0.7, 0.8, 0.9] were examined for Deseasonalized $Landsat_{NDVI}$ ($Landsat_{NDVI}D$), Sentinel-1 with VV polarization ($S1_{VV}$) and combination of the two datasets (Figure 15), to determine the optimal output for section 4.2.

Results for stable forest (F) yield relatively low Producer's (PA) and User's accuracies (UA) for all the three scenarios, although $Landsat_{NDVI}D$ outperforms the other two by a large margin. As expected, the combined scenario largely reflects $S1_{VV}$ accuracies due to the number of valid observations in the dataset used for the analysis (Figure 4).

On contrary, when looking at the disturbed forest (NF) class, UA's and PA's are high for all three scenarios and largely negatively correlated with threshold values (increase of threshold resulted in lower accuracies). Additionally, OA was calculated for mapping the target area.

We compared mean time lags for when the change was first flagged (*Tf*) and when it was confirmed (*Tcon*) for all threshold values of the NF class. First scenario with only $Landsat_{NDVI}D$ showed both, the largest MTL_F as well as MTL. Temporal accuracies for the second and third scenario showed large improvements in MTL_F and MTL, which is a direct result of high number of $S1_{VV}$ valid observations per pixel. Additionally, the absolute difference in days between the two scenarios using $S1_{VV}$ and was twice as low as in the one with only $Landsat_{NDVI}D$.

With the objective to map the damage extent in mangrove forest areas within the shortest possible time lag, trade-off between temporal and spatial component was needed. While the lowest change detection MTL was 10 days for scenarios 2 and 3 (X = 0.5), F class was largely underestimated. Taking into consideration the fact that all the UA's & PA's for NF class exceeded 90%, the decisive parameter was the accuracy result for stable forest UA (Appendix, Table 7). Hence, when examining validation results, we opted for using the identical parameters & datasets for extrapolating methodology as we did for the third scenario with threshold set at 0.9.

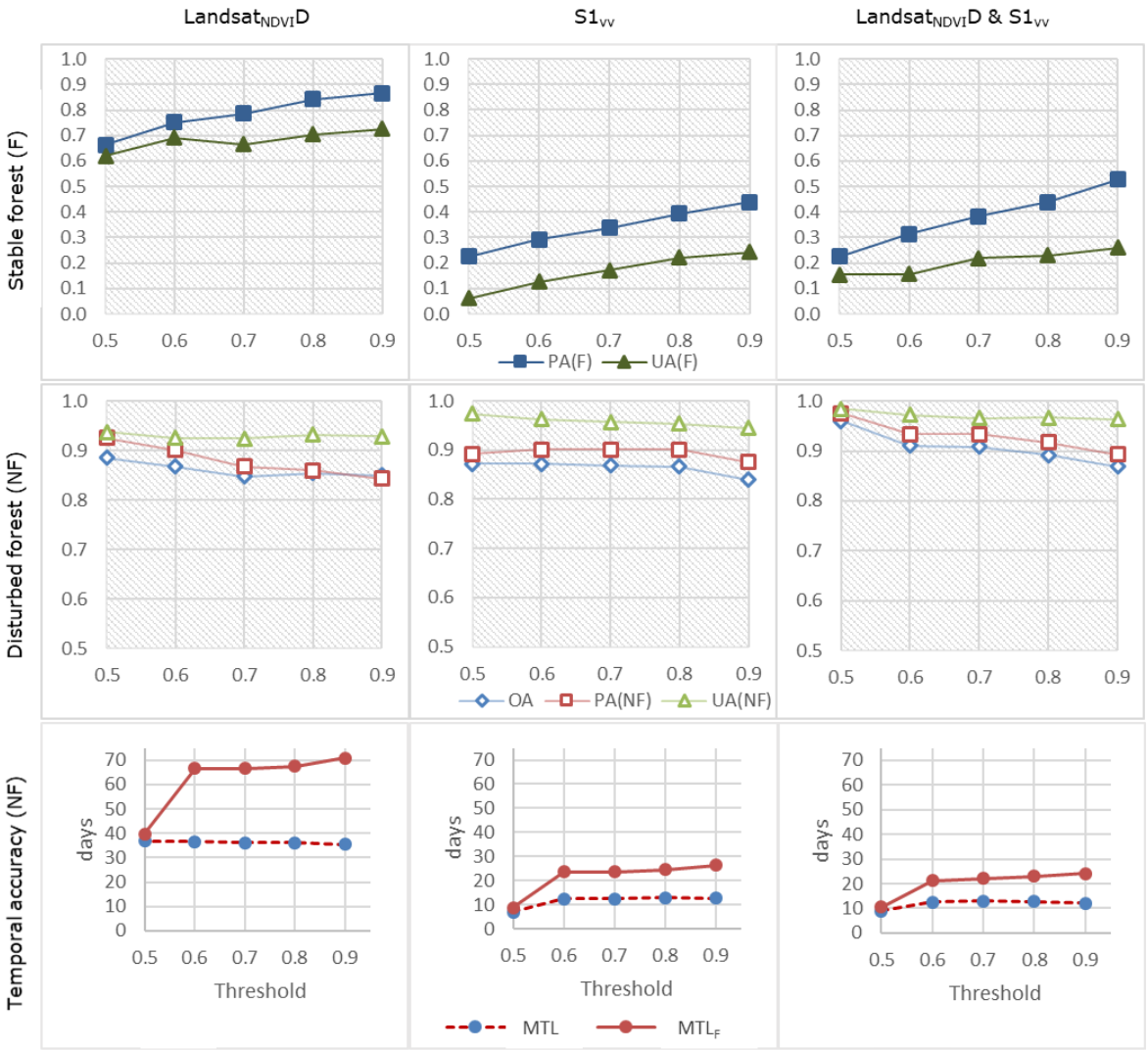

Figure 15: Area adjusted spatial & temporal accuracies for disturbed forest (NF) and stable forest (F) class in case of three scenarios. Upper plots depict spatial accuracy, lower graphs show mean time delay between the disturbance event and disturbance confirmed (MTL) or disturbance flagged (MTL$_F$).

4.2. Upscaling the optimal scenario

Following the accuracy results from section 4.1 from the development area, final map (Figure 16) was produced for a large part of mangrove ecosystems in eastern Viti Levu (study area), applying the methodology from the development area.

In total, 30,410 pixels were labelled as disturbed (NF) and 51,515 as stable forest (F). The latter implies that according to our methodology 37% of mangrove forests experienced disturbance and 63% were left unaffected according to our definition of disturbance (section 1.1). Calculated mean time lag (MTL) of the NF class for the study area was 48 days.

In accordance with the tropical cyclone path (Northern part of Viti Levu; East to West), the Eastern area (Figure 16, subsets 2;3;4) exhibits highest NF proportions per mangrove stand, while the northern stands (1) seem less affected. Here, mangrove stand is considered as clustered pixels of mapped mangroves. Even though the southernmost part (5) was the furthest away from the cyclone path, high number of pixels yield change class (NF).

We compared the derived map with post-disaster high resolution satellite imagery from the 5 chosen areas labelled 1-5 in the map below. All of them largely coincide with our F/NF classification results, except for the southernmost part (5). For each of the 5 above mentioned plots pre and post-disturbance stage imagery is displayed for three sub-areas and overlaid with our F/NF classification product (Appendix, Figures 18-22).

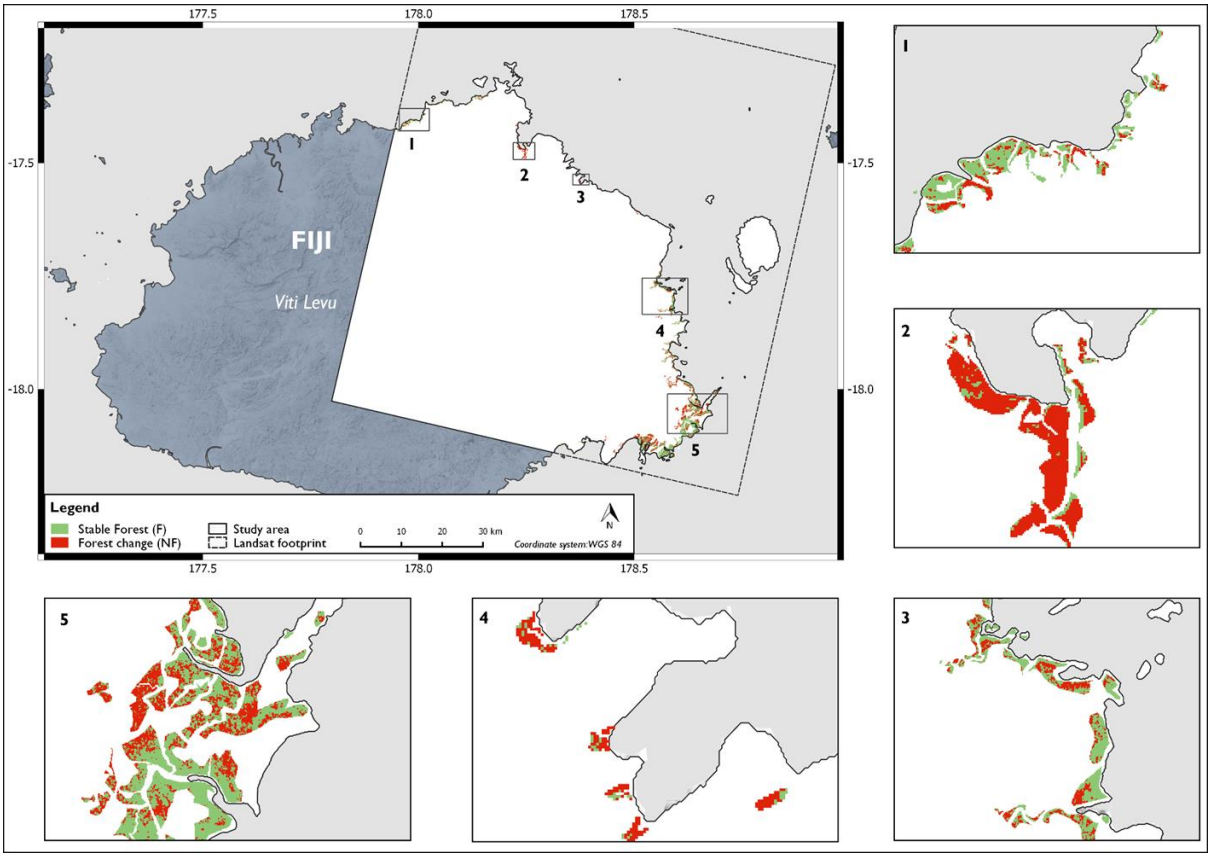

Figure 16: Final map with subsets (1-5) showing the results of Winston Cyclone impact on mangrove ecosystem according to our methodology.

5. Discussion

In this study we presented the feasibility for mangrove forest disturbance monitoring with comparing and integrating time series from Sentinel-1 SAR C-band and Landsat NDVI in our development area. We performed a thorough validation without using any field reference datasets, in order to quantify the accuracy of spatial and temporal components for the results of all the three scenarios (see section 3.1; Methodology flowchart). Later that same methodology was extrapolated to a larger extent (study area).

Investigating trends in pixel-based time series of Sentinel-1 revealed steep increase in backscatter values [5-7 dB] for mangrove ecosystems (see figure 7) following the disturbance event. With C-band SAR, volume scattering is the dominant scattering mechanism in closed canopies. With structural changes in the canopy following the cyclone, volume scattering and double bounce scattering contributed to the above mentioned signal increase in combination with high waters after the cyclone. (Mougin et al.; Kovacs et al. 2008). Furthermore, backscatter retained the high level until the end of the monitoring period. Further research into complex backscatter mechanisms is needed for the improvement of monitoring disturbances with C-band SAR.

Even though mangrove ecosystems are considered evergreen, findings from Agraz Hernández et al. (2011), Zhang et al. (2016), Pastor-Guzman et al. (2018) showed seasonal variability in mangrove ecosystems. Therefore, we decided to evaluate if spatial normalization of the datasets can account for seasonality of mangrove ecosystems in our development area. While LandsatNDVI dataset performed better when we applied the spatial normalization, results for Sentinel-1VV showcased smaller difference between stable forest (F) and disturbed forest (NF) with applied spatial normalization (section 3.4).

However, the separability analysis only demonstrated how good can we differentiate between the selected F/NF sample areas within the development area. Limitation to our methodology was the lack of optional locations for the development area. We focused on choosing an area with clearly distinguishable disturbance in mangrove ecosystems, visible on Pleiades VHR (footprint in figure 2). With the above mentioned criteria, chosen development area was the only possible choice. Hence, we had difficulties in extracting representative PDF's for stable forest inside our development area. Even if the selected sample area appeared as stable forest in the images, the structure of the canopy likely still changed because of the cyclone. Relatively low UA for F could be the result of the described PDF's extraction method. Ideally we would extract PDF's in an area, large enough to contain disturbed forest and stable forest without structural damage.

Combination of spatially normalized optical (LandsatNDVID) and SAR (Sentinel-1VV) time series proved to have the best mean time lag (MTL) for our development area, decreasing disturbance detection time delay in comparison with single sensor time series. LandsatNDVID MTL was at least twice as high and Sentinel-1VV MTL was 1-3 days higher for all selected thresholds. Large part of the improved MTL with combined time series is on the account of the large number of Sentinel-1 valid observations. While the level of information provided by Landsat can be observed when comparing MTL results for combination of the two and Sentinel-1. While timely disturbance detection is essential, trade-off has to be made with the spatial accuracy component. The user has to decide for the most appropriate combination of parameters according to the costs of false positives and false negatives. For example; if one needs a near real time information for immediate damage mitigation or set up an action plan, the threshold should be set at 0.5. The later will result in a decrease in spatial accuracy. On the other hand, if a damage estimation is needed for calculating carbon revenues after an event, threshold should be set at 0.9 to obtain the highest spatial accuracy possible.

Study area (Eastern part of Viti Levu) mangrove forests was mapped with respect to the validation results from all three scenarios. Combined $Landsat_{NDVI}D$ and Sentinel-1 optimal was chosen as the optimal one (threshold = 0.9). The resulting map was compared with high resolution optical imagery taken after the Winston cyclones to see the visual compliance between the two. While areas in the proximity of the development area visually corresponded to the result, mangrove areas in the South-Eastern part of the island were inconsistent with our results. The latter could be a consequence of the difference between mangrove types in different parts of the study area or previously described challenging PDF extraction. Findings from Proisy et al. (2002) showed that difference in mangrove stands structural properties influence SAR C-band backscatter values. In our case, Sentinel-1 inclusion is the most likely the reason for the false negatives in the study area. Our results indicate that using solely $Landsat_{NDVI}D$ dataset would significantly decrease the false detections. However, a-priori knowledge based on field surveys or maps of species communities and zonal patterns would help to calibrate our monitoring system for Sentinel-1 backscatter (Ellison 2015; Kuenzer et al. 2011).

In addition, the majority of the southern Mangrove stands are in the vicinity of urban areas where inhabitants exploit ecosystem resources from mangrove forests on daily basis (Ellison 2015). If we look at our NF class, the pixels of confirmed disturbance generally gravitated towards densely inhabited areas.

6. Conclusion & Future Outlook

This research provided a first step towards developing a near real time disturbance monitoring system for mangrove ecosystems on Fiji. The developed methodology was used for a post-disturbance damage estimation through the case study of Winston cyclone.

We showed how the disturbance event reflected in optical and SAR time series before and after the event. We applied spatial normalizatization to both datasets to account for seasonality in mangrove ecosystem. We compared how convenient the results are as the inputs to the designed monitoring system through the separability analysis. In comparison with the original datasets, Jeffries-Matusita distance was higher for spatially normalized LandsatNDVI and lower for spatially normalized Sentinel-1. We proceeded with the two best options (normalized Landsat and original S-1) and combined them through a probabilistic approach for disturbance detection. Furthermore, we used and adapted methodology from Olofsson et al. (2014) to estimate spatial and temporal accuracy of the detected disturbances and created our own reference dataset without any field data. The latter can be applied for any area, where we have (freely) available high resolution imagery. After calculating the accuracies, we chose the optimal parameters to extrapolate our methodology and test the monitoring system on a larger extent and estimate the damage. According to us, 37% of mangrove ecosystems experienced disturbance and the mean time detection delay was 48 days. We demonstrated how the designed system benefits from combining datasets from optical and SAR sensors – timely detection and higher spatial accuracy compared to single sensors.

The advantage of the methodology designed in our research is the capacity to integrate inputs of multiple optical and radar data sources with compliant geometries (e.g. Sentinel-1 C-band SAR, ALOS PalSAR L-band SAR, Sentinel-2, Landsat) with little effort and required inputs (pre-processed, co-registered datasets, accurate mangrove mask and reliable sample areas for extracting PDF's). Robustness of the system at the same time allows for monitoring disturbances in other types of tropical forests.

Further research is needed to exploit the full potential of the designed monitoring system. First step should be implementing the methodology in a separate mangrove habitat with reliable locations of disturbed and stable forest and a field dataset, describing the structural damage on mangrove ecosystems for a number of forest plots. The later would help us with further understanding of the two datasets, used in the research. The spatial normalization needs to be further investigated for Sentinel-1 in combination with quantifying the increase in backscatter we discussed earlier in the thesis.

Including Sentinel-2 Multispectral systems (MSI) dataset should be considered as an input to the monitoring system. Sentinel-2 MSI provides high spatial resolution imagery with the revisit time of 5 days and unique characteristics for vegetation mapping (Clerici et al. 2017; Delegido et al. 2011).

References

Agraz Hernández, C., García Zaragoza, C., Iriarte-Vivar, S., Flores-Verdugo, F., Moreno Casasola, P. (2011). Forest structure, productivity and species phenology of mangroves in the La Mancha lagoon in the Atlantic coast of Mexico. Wetlands Ecology and Management 19(3): 273-293.

Alongi, D. (2008). Mangrove forests: resilience, protection from tsunamis, and responses to global climate change. Estuarine Coastal and Shelf Science 76: 1–13.

Ash, J. (1992). Vegetation ecology of Fiji: past, present, and future perspectives. Pacific Science 46: 111-127.

Atkinson, S., Jupiter, S., Adams, V., Carter Ingram, J., Narayan, S., Klein, C., Possingham, H. (2016). Prioritising Mangrove Ecosystem Services Results in Spatially Variable Management Priorities. PloS one 11 (3): e0151992.

Barbier, E. (2007). Valuing ecosystem services as productive inputs. Economic Policy 22(49): 177-229.

Bogoliubova A., Tymków P. (2014). Accuracy assessment of automatic image processing for land cover classification of St. Petersburg protected area. Acta Scientiarum Polonorum Geodesia et Descriptio Terrarum 13 (1-2): 5–22.

Brander, L., Wagtendonk, A., Hussain, S., McVittie, A., Verburg, P., Groot, R., Ploeg, S. (2012). Ecosystem service values for mangroves in Southeast Asia: A meta-analysis and value transfer application. Ecosystem Services 1(1): 62-69.

Calderucio, G., Estrada, D., Luiz, M., Fernadez, V., Almeida, P. (2014). The economic evaluation of carbon storage and sequestration as ecosystem services of mangroves: a case study from southeastern Brazil. International Journal of Biodiversity Science, Ecosystem Services & Management 11(1): 29-35.

Chen, F. (2016). Deforestation monitoring in the Amazon River estuary by multi-temporal Envisat ScanSAR data. IOP Conference Series: Earth and Environmental Science 34: 012003.

Clerici, N., Valbuena Calderón, C. & Posada, J. (2017) Fusion of Sentinel-1A and Sentinel-2A data for land cover mapping: a case study in the lower Magdalena region, Colombia. Journal of Maps 13(2): 718-726.

Cohen, W.B., Yang, Z., Kennedy, R.E. (2010). Detecting trends in forest disturbance and recovery using yearly Landsat time series: 2. TimeSync – Tools for calibration and validation. Remote Sensing of Environment 114: 2911 – 2924.

Cohen, W.B., Healey, S.P., Yang, Z., Stehman, S.V., Brewer, C.K., Brooks, E.B., Gorelick, N., Huang, C., Hughes, M.J., Kennedy, R.E., Loveland, T.R., Moisen, G.G., Schroeder, T.A., Vogelmann, J.E., Woodcock, C.E., Yang, L., Zhu, Z. (2017). How similar are forest disturbance maps derived from different Landsat time series algorithms? Forests 8(4): 1-19.

Cornforth, A., Fatoyinbo, E., Freemantle, P., Pettorelli, N. (2013). Advanced Land Observing Satellite Phased Array Type L-Band SAR (ALOS PALSAR) to Inform the Conservation of Mangroves: Sundarbans as a Case Study. Remote Sensing 5: 224-237.

Danielsen, F., Sørensen, M., Olwig, M., Selvam, V., Parish, F., Burgess, N., Hiraishi, T. et al. (2005). The Asian tsunami: A protective role for coastal vegetation. Science 310(5748): 643.

Das, S., Vincent, J.R. (2009). Mangroves protected villages and reduced death toll during Indian super cyclone. Proceedings of the National Academy of Sciences of the United States of America 106(18): 7357-7360.

De Oliveira Pereira, L., Da Costa Freitas, C., Anna, S., Lu, D., Moran, E. (2013). Optical and radar data integration for land use and land cover mapping in the Brazilian Amazon. GIScience and Remote Sensing 50: 301-321.

De Sy, V., Herold, M., Achard, F., Asner, G., Held, A., Kellndorfer, J., Verbesselt, J. (2012). Synergies of multiple remote sensing data sources for REDD+ Monitoring. Current Opinion in Environmental Sustainability 4: 696 - 706.

Delegido, J., Verrelst, J., Alonso, L., & Moreno, J. (2011). Evaluation of Sentinel-2 red-edge bands for empirical estimation of green LAI and chlorophyll content. Sensors 11:7063–7081.

Di Liberto, T. (2016). Tropical Cyclone Winston causes devastation in Fiji, a tropical paradise. URL:https://www.climate.gov/news-features/event-tracker/tropical-cyclone-winston-causes-devastation-fiji-tropical-paradise.

Ellison, J. (2015) Vulnerability assessment of mangroves to climate change and sea-level rise impacts. Wetlands Ecology and Management 23(2): 115-137.

FAO (2007): The world's mangroves 1980-2005. FAO Forestry paper 153. URL: http://www.fao.org/docrep/010/a1427e/a1427e00.htm.

FAO (2016): Map Accuracy Assessment and Area Estimation: A Practical Guide. National forest monitoring assessment working paper 46: 60.

Ghosh, D. (2011). Mangroves: The most fragile ecosystem. Resonance 16(1): 47–60.

Global Forest Resources Assessment 2000 (2001). URL:ftp://ftp.fao.org/docrep/fao/003/y1997e/fra%202000%20main%20report.pdf .

Giri, C., Ochieng, E., Tieszin, L. L., Zhu, Z., Singh, A., Loveland, Masek, T. J., Duke, N. (2011). Status and distribution of mangrove forests of the world using earth observation satellite data. Global Ecology and Biogeography 20: 154-159.

Granek, E., Ruttenberg, B. (2007). Protective Capactiy of Mangroves During Tropical Storms: A Case Study from 'Wilma' and 'Gamma' in Belize. Marine Ecology-progress Series 343: 101-105.

Griffiths, P. (2015). Forest cover dynamics during massive ownership changes – annual disturbance mapping using annual Landsat time-series. Remote Sensing Time Series: Revealing Land Surface Dynamics 22: 307-322.

Hamunyela, E. (2017). Space-time monitoring of tropical forest changes using observations from multiple satellites (doctoral dissertation). Wageningen University, Wageningen, Netherlands.

Hamunyela, E., Verbesselt, J., Herold, M. Using spatial context to improve early detection of deforestation from Landsat time series.Remote Sensing of Environment 172: 126–138

Herold, N., Haack, B. (2008). Comparison and Integration of Radar and Optical Data for Land Use/Cover Mapping. Geocarto International 21: 9-18.

Hieu, P., Dung Luu, V., Nguyen, T., Koji, O.(2017). Will restored mangrove forests enhance sediment organic carbon and ecosystem carbon storage? Regional Studies in Marine Science 14: 43-52.

Kanniah, K., Sheikhi, A., Cracknell, A., Goh, H., Tan, K., Ho, C., Rasli, F. (2015). Satellite images for monitoring mangrove cover changes in a fast growing economic region in southern Peninsular Malaysia. Remote Sensing 7: 14360–14385.

Kasischke, E., Melack, J., Dobson, C. (1997). The use of imaging radars for ecological applications—A review. Remote Sensing of Environment 59(2): 141-156.

Kovacs, J., Vandenberg, C., Flores-Verdugo, F. (2006). Assessing fine beam RADARSAT-1 backscatter from a white mangrove (Laguncularia racemosa (Gaertner)) canopy. Wetlands Ecology Management 14(5): 401-408.

Kovacs, J., Vandenberg, C., Wang, J., Flores-Verdugo, F. (2008). The Use of multipolarized spaceborne SAR backscatter for monitoring the health of a degraded mangrove forest. Journal of Coastal Research 24(1): 248-254.

Kuenzer, C., Bluemel, A., Gebhardt, S., Quoc T. V., Dech, S. (2011). Remote Sensing of Mangrove Ecosystems: A Review. Remote Sensing 3(5): 878-928.

Le Page, M. (2016). Record global temperatures bring strongest ever cyclone to Fiji. URL:https://www.newscientist.com/article/2078365-record-global-temperatures-bring-strongest-ever-cyclone-to-fiji/

Lehmann, A. (2015). SAR and optical remote sensing: Assessment of complementarity and interoperability in the context of a large-scale operational forest monitoring system. Remote Sensing of Environment 156: 335-348.

Long, J., Napton, D., Chandra, G., Graesser, J. (2013). A Mapping and Monitoring Assessment of the Philippines' Mangrove Forests from 1990 to 2010. Journal of Coastal Research 30(2): 260–271.

Lugo, A. E. (2008). Visible and invisible effects of hurricanes on forest ecosystems: an international review. Austral Ecology 33: 368 – 398.

McNairn, H., Champagne, C., Shang, J., Holmstrom, D., Reichert, G. (2009). Integration of optical and Synthetic Aperture Radar (SAR) imagery for delivering operational annual crop inventories. ISPRS Journal of Photogrammetry and Remote sensing 64: 434-449.

Mitchell, A., Tapley I., Milne, A., Williams, M., Zhou, Z., Lehmann, E., Caccetta, P., Lowell, K., Held, A. (2014). C- and L-band interoperability: Filling the gaps in continuous forest cover mapping in Tasmania. Remote Sensing of Environment 155: 58-68.

Mougin, E., Proisy, C., Marty, G., Fromard, F., Puig, H., Betoulle, J., Rudant, J. (1999). Multifrequency and multipolarization radar backscattering from mangrove forests. IEEE Transactions on Geoscience and Remote Sensing, 37(1): 94-102.

Nagler, T. (2015). The Sentinel-1 Mission: New Opportunities for Ice Sheet Observations. Journal Remote Sensing 7: 9371 - 9389.

Negron-Juarez, R. (2014). Multi-scale sensitivity of Landsat and MODIS to forest disturbance associated with tropical cyclones. Remote Sensing of Environment 140: 679 - 689.

Olofsson, P., Torchinava, P., Woodcock, C., Baccini, A., Houghton, R., Ozdogan, M. et al. (2010). Implications of land use change on the national terrestrial carbon budget of Georgia. Carbon Balance and Management 5: 4.

Olofsson, P., Kuemmerle, T., Griffiths, P., Knorn, J., Baccini, A., Gancz, V. et al. (2011). Carbon implications of forest restitution in post-socialist Romania. Environmental Research Letters 6: 045202.

Olofsson, P., Foody, G., Herold, M., Stehman, S., Woodcock, C., Wulder, M. (2014). Good practices for estimating area and assessing accuracy of land change. Remote Sensing of Environment 148: 42-52.

Pastor-Guzman, J., Dash, J., Atkinson, P. (2018). Remote sensing of mangrove forest phenology and its environmental drivers. Remote Sensing of Environment 205: 71-84.

Proisy, C., Mougin, E., Fromard, F., Trichon, V., Karam, M. (2002). On the influence of canopy structure on the radar backscattering mangrove forests. International Journal of Remote Sensing 23(20): 4197-4210.

Proisy, C., Mitchell, A., Lucas, R., Fromard, F., Mougin, E. (2003). Estimation of Mangrove Biomass using Multifrequency Radar Data. Application to Mangroves of French Guiana and Northern Australia. Proceedings of the Mangrove Conference, Salvador, Bahia, Brazil, 20–24 May 2003.

Purnamasayangsukasih, R., Norizah, K., Ismail, A, & Shamsudin, I. (2016). A review of uses of satellite imagery in monitoring mangrove forests. IOP Conference Series: Earth and Environmental Science 37(1): 012034.

Ramsar Convention on Wetlands (2013). URL: http://www.ramsar.org/sites/default/files/documents/library/manual6-2013-e.pdf.

Reiche, J., de Bruin, S., Hoekman, D., Verbesselt, J., Herold, M. (2015). A Bayesian Approach to Combine Landsat and ALOS PALSAR Time Series for Near Real-Time Deforestation Detection. Remote Sensing 7(5): 4973 – 4996.

Reiche, J. (2015). Fusing Landsat and SAR time series to detect deforestation in the tropics. Remote Sensing of Environment 156: 276-293.

Reiche, J. (2016). Combining satellite data for better tropical forest monitoring. Nature Climate Change 6: 120.

Sheoran, A., Haack, B. (2013). Optical and radar data comparison and integration: Kenya example. Geocarto International 29: 370-382.

Spalding, M., Kanuma, M., Collins, L., (2010). World Atlas of Mangroves. Earthscan, London.

Thomas, N., Lucas, R., Itoh, T., Simard, M., Fatoyinbo, L., et al. (2015). An approach to monitoring mangrove extents through time-series comparison of JERS-1 SAR and ALOS PALSAR data. Wetlands Ecology and Management 23(1): 3-17.

Torres, J. (2012). GMES Sentinel-1 mission. Remote Sensing of Environment 120: 9-24.

Verbesselt, J., Zeileis, A., Herold, M. (2012). Near real-time disturbance detection using satellite image time series. Remote Sensing of Environment 123: 98-108.

Zhang, K., Thapa, B., Ross, M., Gann, D. (2016). Remote sensing of seasonal changes and disturbances in mangrove forest: a case study from South Florida. Ecosphere 7(6): 1-23.

Zhang, X., Wang, J., Jiang, H. (2013). Remote-sensing assessment of forest damage by Typhoon Saomai and its related factors at landscape scale. International Journal of Remote Sensing 34: 7874-7886.

Ward, R., Friess, D., Day, R., MacKenzie, R. (2016). Impacts of climate change on mangrove ecosystems: a region by region overview. Ecosystem Health and Sustainability 2(4): e01211.

Woodhouse, I. (2006). Introduction to Microwave Remote Sensing. Taylor & Francis group, 355 pp.

Appendix

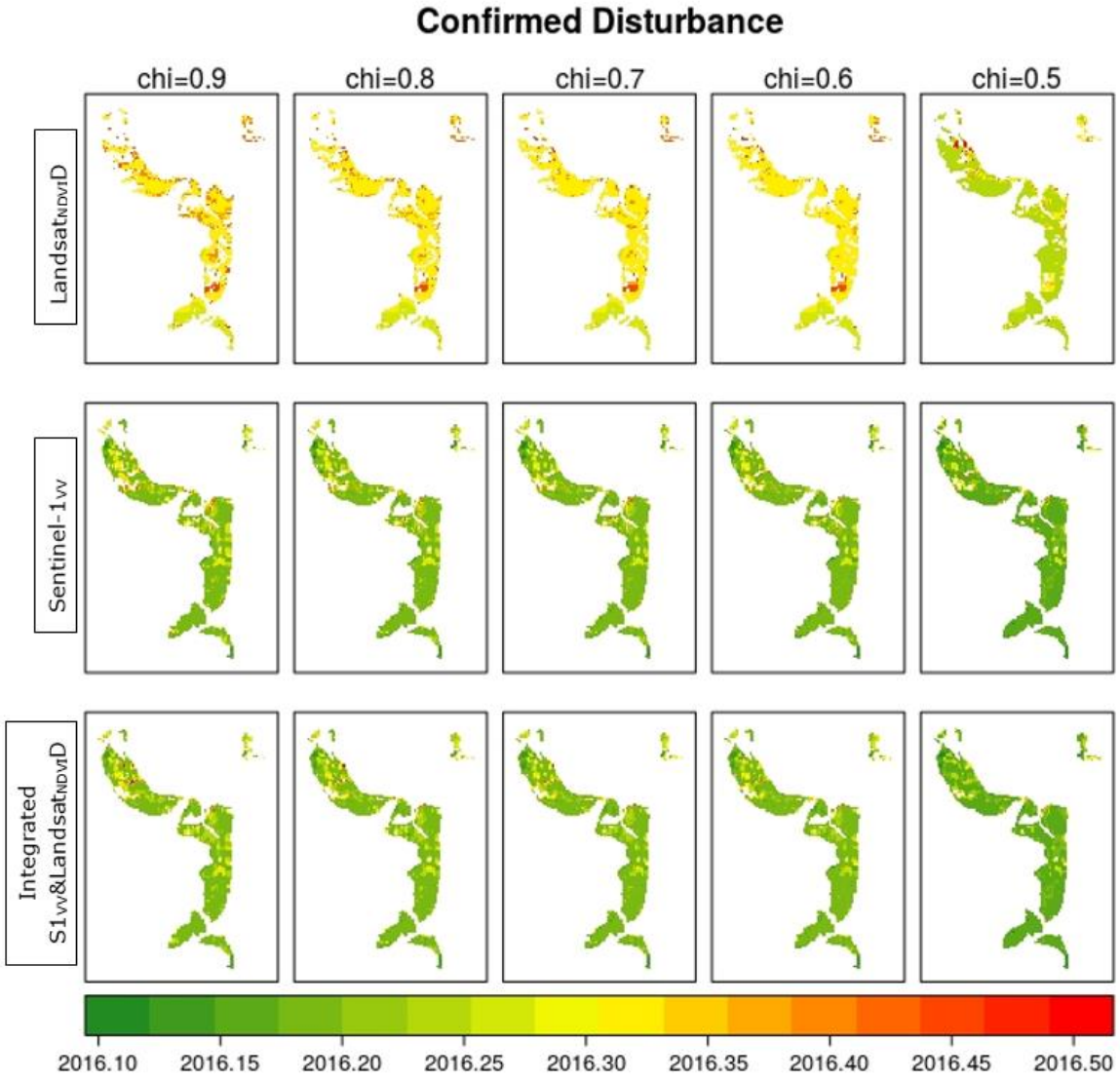

Figure 17: Confirmed disturbances (NF) for our study area. Mangroves, where there was no confirmed change were give NA values.

Validation samples stable forest			n=89
cell	x	y	REF
4783	631545	8068115	0
4556	630915	8068175	0
4555	630885	8068175	0
1325	632865	8069135	0
4893	631755	8068085	0
4451	630855	8068205	0
2456	632805	8068805	0
5433	632505	8067935	0
4792	631815	8068115	0
2457	632835	8068805	0
8421	632535	8067065	0
5730	632145	8067845	0
4241	630735	8068265	0
1659	630525	8069015	0
8106	632355	8067155	0
12406	631575	8065895	0
1660	630555	8069015	0
4554	630855	8068175	0
8318	632535	8067095	0
2563	632925	8068775	0
8004	632385	8067185	0
843	630765	8069255	0
12201	631605	8065955	0
2354	632835	8068835	0
5401	631545	8067935	0
4894	631785	8068085	0
3626	630825	8068445	0
6544	631845	8067605	0
4553	630825	8068175	0
12405	631545	8065895	0
11397	632205	8066195	0
4349	630885	8068235	0
4240	630705	8068265	0
4449	630795	8068205	0
2565	632985	8068775	0
4656	630825	8068145	0
2045	632835	8068925	0
4550	630735	8068175	0
1736	632835	8069015	0
733	630555	8069285	0
4243	630795	8068265	0
2566	633015	8068775	0
4450	630825	8068205	0
3012	630945	8068625	0
12303	631575	8065925	0
5537	632535	8067905	0
5538	632565	8067905	0
12631	632145	8065835	0
2589	630615	8068745	0
4140	630795	8068295	0

Validation samples stable forest			
cell	x	y	REF
6540	631725	8067605	0
4350	630915	8068235	0
4675	631395	8068145	0
3422	630885	8068505	0
8929	632325	8066915	0
2489	630705	8068775	0
2594	630765	8068745	0
2698	630795	8068715	0
2490	630735	8068775	0
7803	632535	8067245	0
3631	630975	8068445	0
3633	631035	8068445	0
7999	632235	8067185	0
6755	631995	8067545	0
4579	631605	8068175	0
3730	630855	8068415	0
2283	630705	8068835	0
5534	632445	8067905	0
5725	631995	8067845	0
7902	632415	8067215	0
12407	631605	8065895	0
6977	632475	8067485	0
2491	630765	8068775	0
5724	631965	8067845	0
4678	631485	8068145	0
5623	632025	8067875	0
5195	631545	8067995	0
8317	632505	8067095	0
10062	632325	8066585	0
10985	632205	8066315	0
4673	631335	8068145	0
6436	631695	8067635	0
3521	630765	8068475	0
7081	632505	8067455	0
2353	632805	8068835	0
6440	631815	8067635	0
3528	630975	8068475	0
7183	632475	8067425	0
4245	630855	8068265	0

Table 5: Reference samples Stable forest

Validation samples disturbed forest			n=121
cell	x	y	REF
8830	632445	8066945	1
5076	631065	8068025	1
10782	632295	8066375	1
5430	632415	8067935	1
5179	631065	8067995	1
3726	630735	8068415	1
5495	631275	8067905	1
4359	631185	8068235	1
6447	632025	8067635	1
8923	632145	8066915	1
3930	630675	8068355	1
4252	631065	8068265	1
4873	631155	8068085	1
5947	632475	8067785	1
12742	632385	8065805	1
7185	632535	8067425	1
7181	632415	8067425	1
6445	631965	8067635	1
5393	631305	8067935	1
6663	632325	8067575	1
13777	632535	8065505	1
5938	632205	8067785	1
5185	631245	8067995	1
7797	632355	8067245	1
13262	632535	8065655	1
1464	630855	8069075	1
10681	632355	8066405	1
4763	630945	8068115	1
6044	632295	8067755	1
6868	632295	8067515	1
5322	632265	8067965	1
2691	630585	8068715	1
4153	631185	8068295	1
5735	632295	8067845	1
2391	630855	8068805	1
9541	632145	8066735	1
2690	630555	8068715	1
5085	631335	8068025	1
3933	630765	8068355	1
2598	630885	8068745	1
4886	631545	8068085	1
10786	632415	8066375	1
5738	632385	8067845	1
5841	632385	8067815	1
6760	632145	8067545	1
12305	631635	8065925	1
6151	632415	8067725	1
10576	632295	8066435	1
5527	632235	8067905	1
12516	631785	8065865	1
7179	632355	8067425	1
8417	632415	8067065	1
11398	632235	8066195	1
11195	632325	8066255	1
10675	632175	8066405	1
5284	631125	8067965	1
9131	632205	8066855	1
11393	632085	8066195	1
6976	632445	8067485	1
5531	632355	8067905	1
8209	632355	8067125	1
10889	632415	8066345	1
5190	631395	8067995	1
11399	632265	8066195	1
4993	631665	8068055	1

Validation samples disturbed forest			
cell	x	y	REF
12317	631995	8065925	1
10370	632295	8066495	1
6144	632205	8067725	1
6146	632265	8067725	1
9959	632325	8066615	1
5949	632535	8067785	1
5417	632025	8067935	1
7900	632355	8067215	1
2803	630855	8068685	1
10473	632295	8066465	1
10163	632265	8066555	1
3103	630585	8068595	1
4250	631005	8068265	1
11297	632295	8066225	1
4787	631665	8068115	1
13365	632535	8065625	1
4879	631335	8068085	1
5186	631275	8067995	1
11087	632175	8066285	1
6554	632145	8067605	1
6762	632205	8067545	1
6660	632235	8067575	1
9339	632265	8066795	1
2791	630495	8068685	1
4885	631515	8068085	1
8627	632535	8067005	1
7590	632325	8067305	1
6352	632265	8067665	1
4033	630675	8068325	1
10573	632205	8066435	1
6667	632445	8067575	1
5837	632265	8067815	1
5389	631185	8067935	1
9141	632505	8066855	1
1219	632775	8069165	1
12426	632175	8065895	1
7589	632295	8067305	1
6462	632475	8067635	1
2798	630705	8068685	1
1940	632775	8068955	1
10367	632205	8066495	1
4985	631425	8068055	1
4981	631305	8068055	1
6344	632025	8067665	1
5117	632295	8068025	1
1250	630615	8069135	1
3835	630915	8068385	1
12330	632385	8065925	1
2564	632955	8068775	1
2665	632895	8068745	1
4786	631635	8068115	1
4662	631005	8068145	1
2462	632985	8068805	1
5525	632175	8067905	1
2664	632865	8068745	1
11997	631665	8066015	1

Table 6: Reference samples Disturbed forest.

	threshold (X)	MTLF	MTL	OA	PA(NF)	UA(NF)	PA(F)	UA(F)
$L8_{NDVI}D$	0.9	35	71	0.85	0.84	0.93	0.87	0.73
	0.8	36	68	0.85	0.86	0.93	0.84	0.70
	0.7	36	67	0.85	0.87	0.92	0.79	0.67
	0.6	37	66	0.87	0.90	0.93	0.75	0.69
	0.5	37	40	0.89	0.93	0.94	0.66	0.62
$S\text{-}1_{VV}$	0.9	13	26	0.84	0.88	0.95	0.44	0.24
	0.8	13	25	0.87	0.90	0.95	0.39	0.22
	0.7	13	24	0.87	0.90	0.96	0.34	0.17
	0.6	13	24	0.87	0.90	0.96	0.29	0.13
	0.5	7	9	0.87	0.89	0.97	0.22	0.06
$S1_{VV}\&L8_{NDVI}D$	0.9	12	24	0.87	0.89	0.96	0.53	0.26
	0.8	13	23	0.89	0.92	0.97	0.44	0.23
	0.7	13	22	0.91	0.93	0.97	0.38	0.22
	0.6	13	21	0.91	0.93	0.97	0.31	0.16
	0.5	9	11	0.96	0.98	0.98	0.22	0.15

Table 7: Area adjusted Accuracies for Thresholds [0.5-0.9] for all the three scenarios, including MTLF (mean time lag of the flagged change) and MTL (mean time lag of the confirmed change).

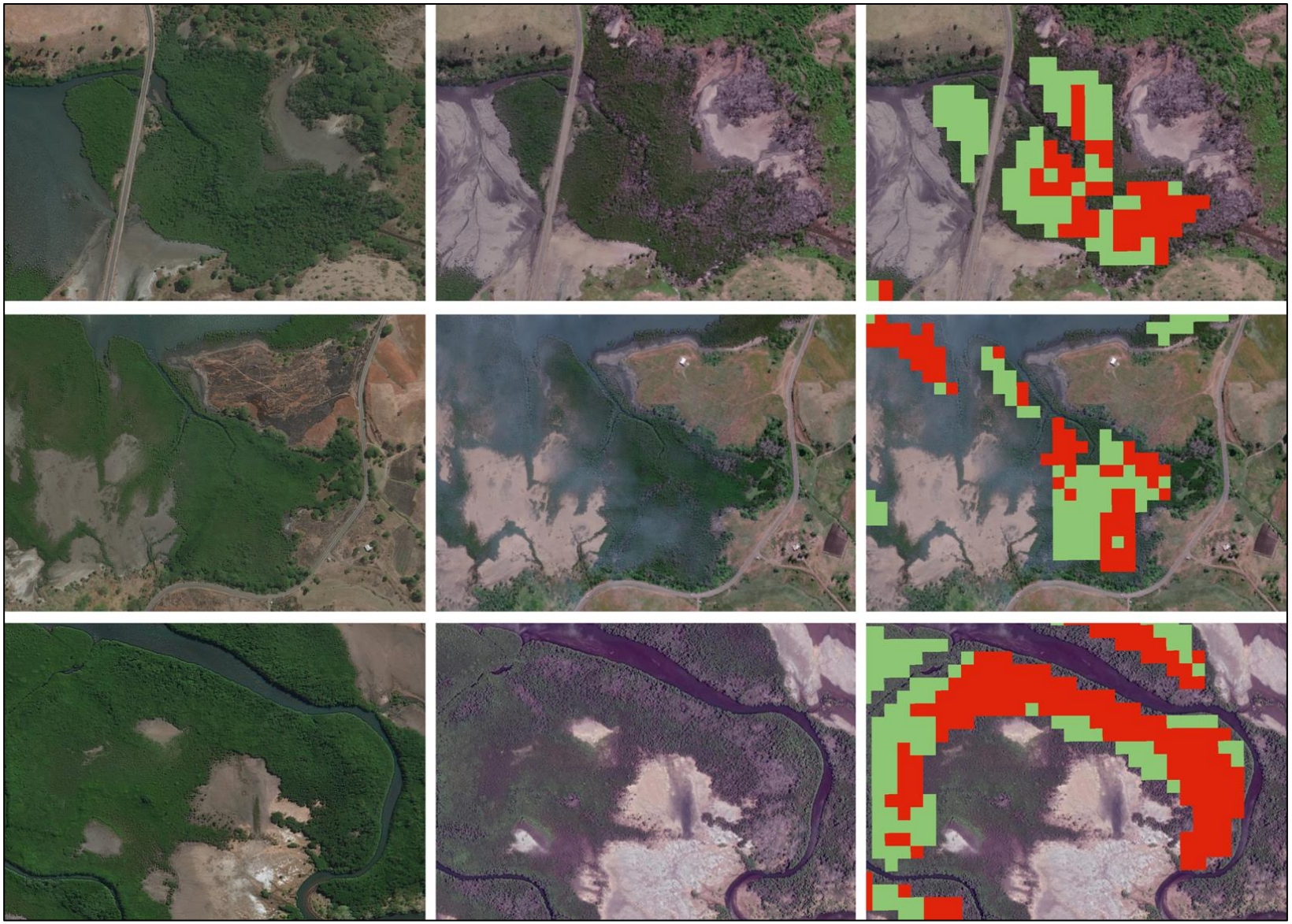

Figure 18: Section 1: High resolution imagery taken before and after the Winston Cyclone and overlay with our results.

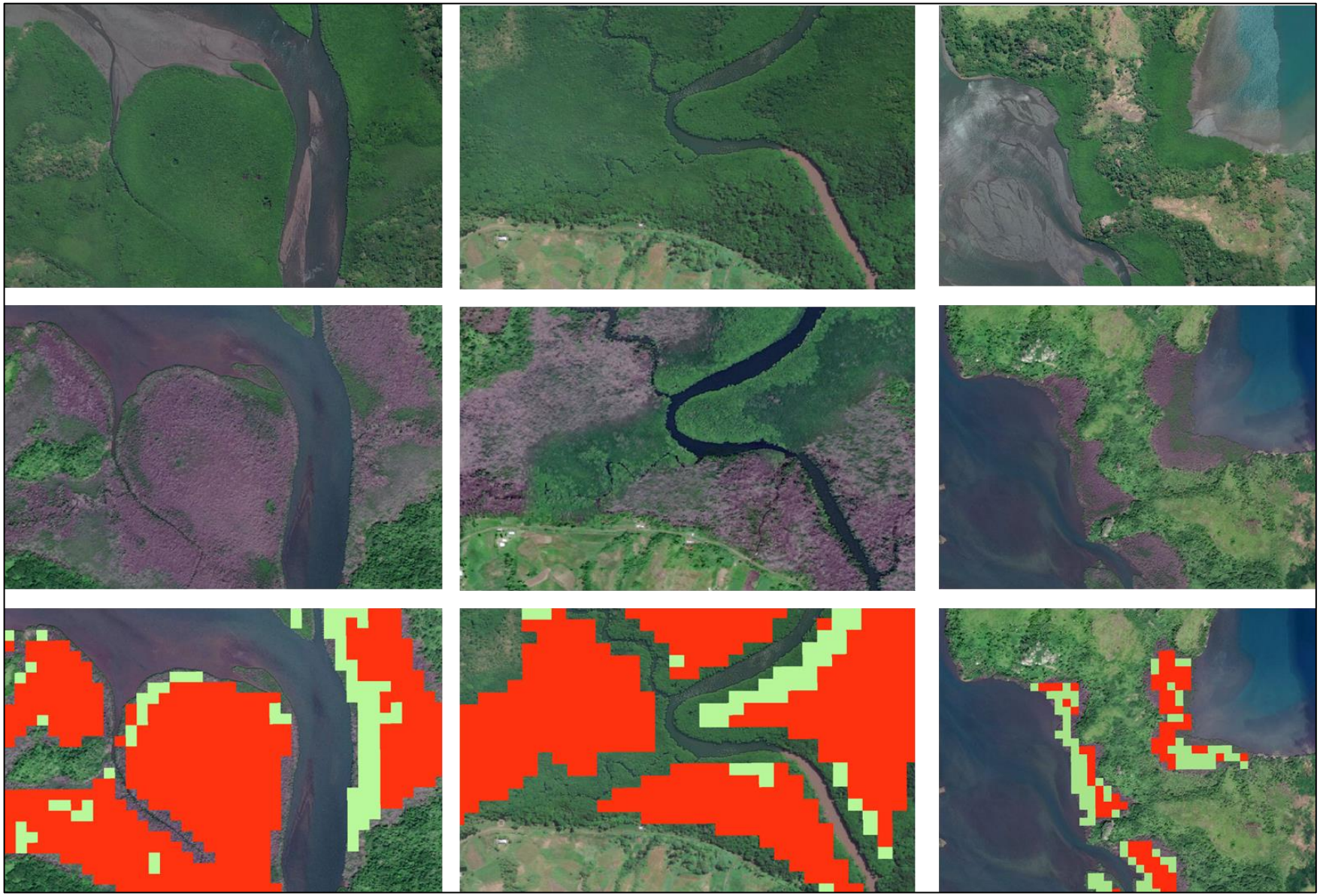

Figure 19: Section 2: High resolution imagery taken before and after the Winston Cyclone and overlay with our results

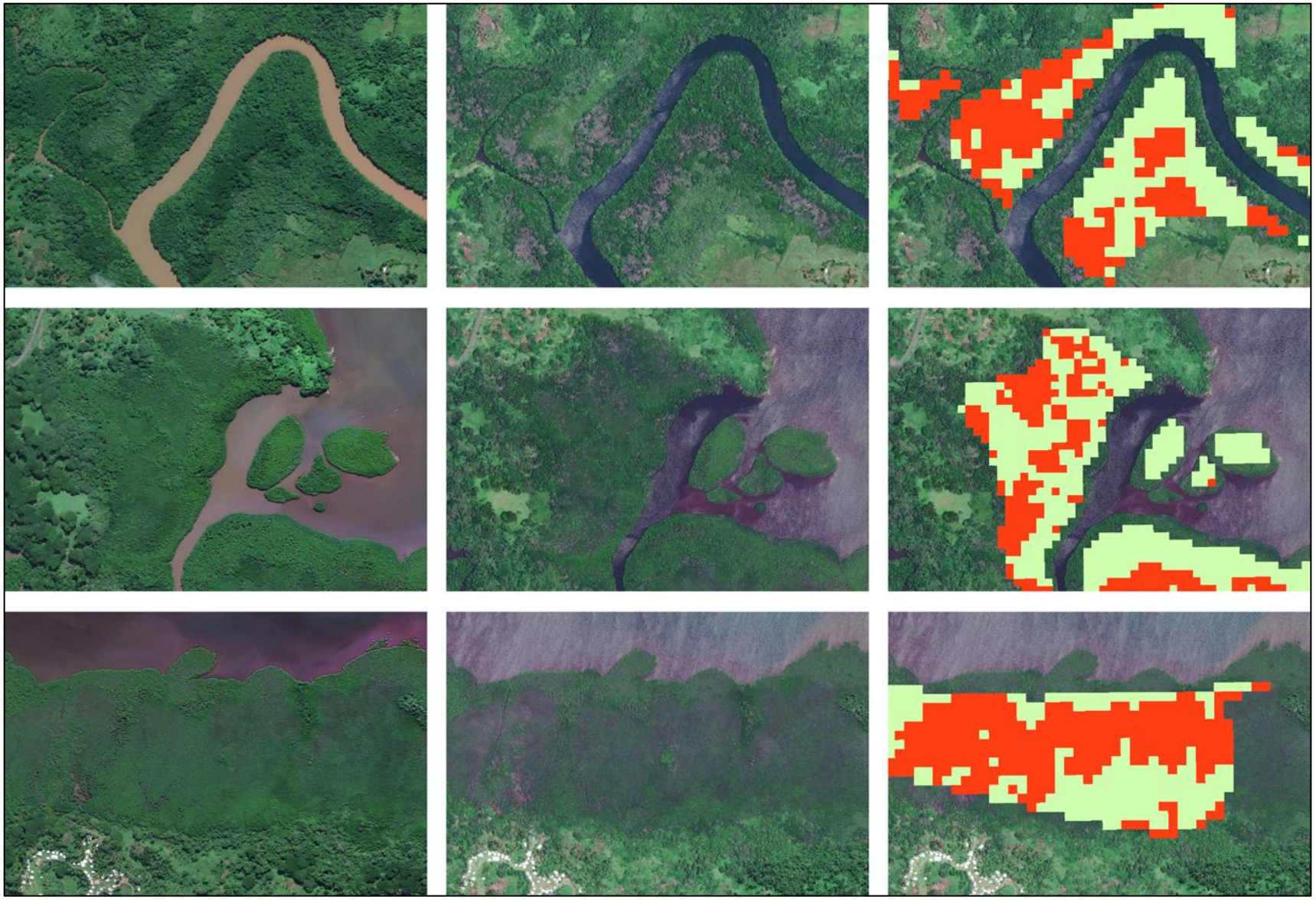

Figure 20: Section 3: High resolution imagery taken before and after the Winston Cyclone and overlay with our results.

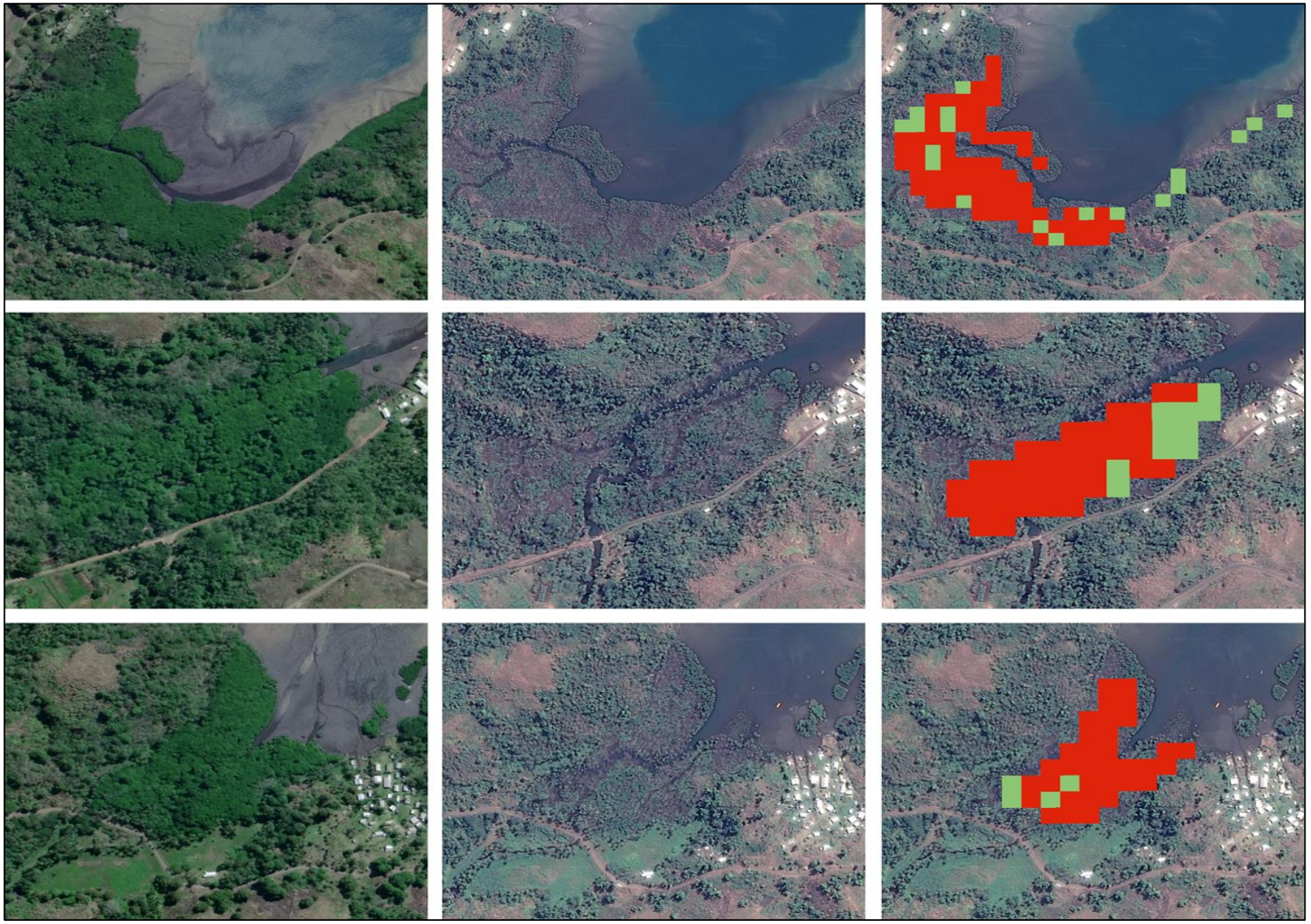

Figure 21: Section 4: High resolution imagery taken before and after the Winston Cyclone and overlay with our results.:

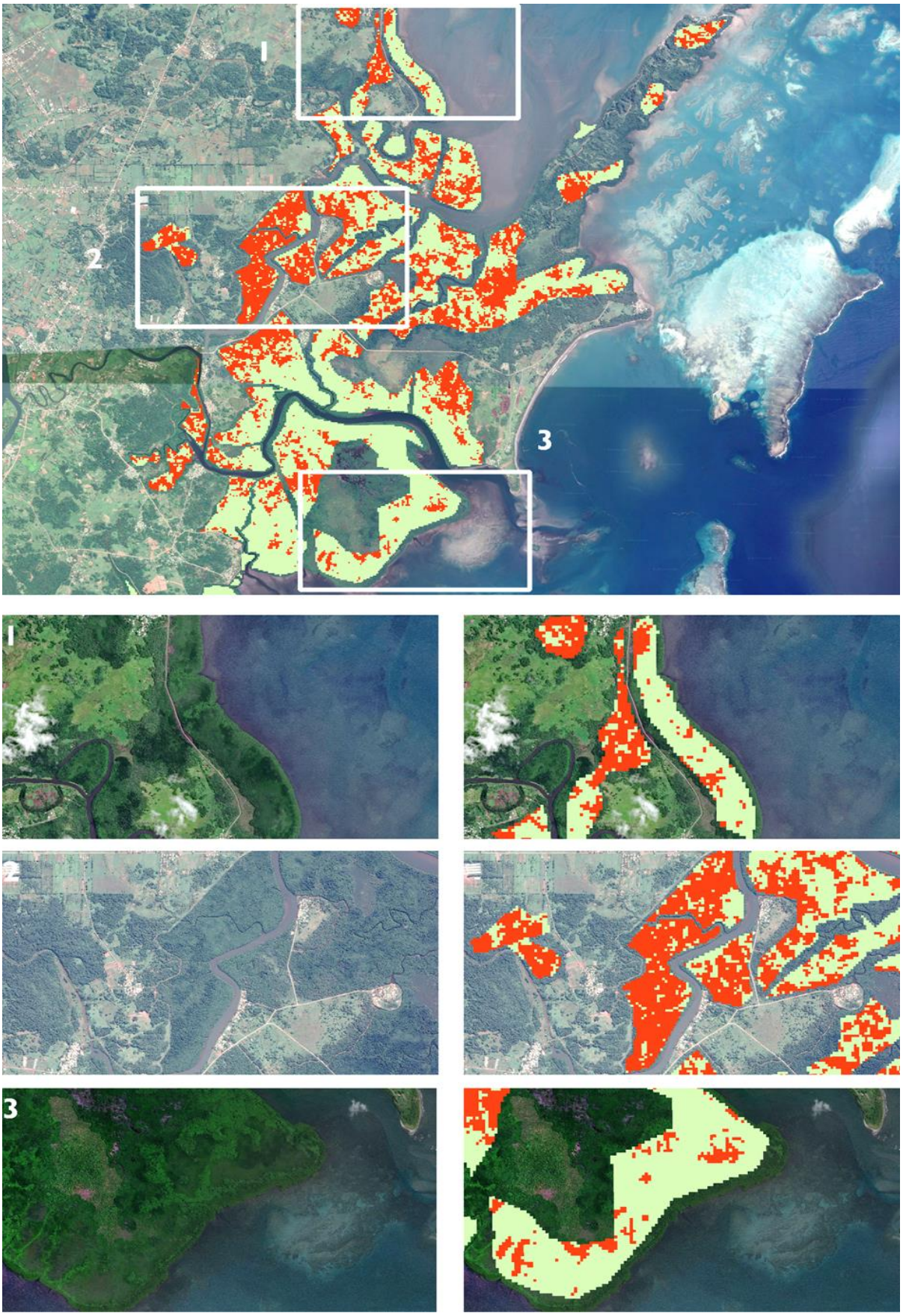

Figure 22: Section 5: High resolution imagery taken after the Winston Cyclone and overlay with our results